FCS-MPC of Power Converters: A Data-Driven Model-Free Reinforcement Learning Solution

Xing Liu, *Senior Member, IEEE*, Lin Qiu, *Senior Member, IEEE*, Youtong Fang, *Senior Member, IEEE*, Kui Wang, *Senior Member, IEEE*, Yongdong Li, *Senior Member, IEEE*, and Jose Rodríguez, *Life Fellow, IEEE*

***Abstract*—This article builds the theoretical foundations for finite-control set model predictive control by leveraging the theory of data-driven model-free reinforcement learning solution. Specifically, the philosophy behind the proposed control methodology relies on the conjunction of developing a proportional–integral-like data-driven dynamic internal model predictive control, deploying a reinforcement learning technique, and introducing a variable-step event-driven mechanism. The present research provides a new avenue and overcomes known shortcomings of finite-control set model predictive control relating to its model-plant mismatch and its application to limitations with unknown external disturbances and unnecessary commutation actions. Finally, through extensive numerical examples, we illustrate our findings and highlight its merits, and the results presented are promising to reject both model mismatch and unknown disturbances and motivate further research in this field.**

Received 22 June 2025; revised 13 September 2025 and 11 November 2025; accepted 2 December 2025. Date of publication 11 December 2025; date of current version 25 February 2026. This work was supported in part by the National Natural Science Foundation of China under Grant 52577218, in part by the State Key Laboratory of Power Transmission Equipment Technology through Open Research Project under Grant SKLPET-kfkt202406, in part by the State Key Laboratory of High-speed Maglev Transportation Technology under Grant SKLM-SFCF-2023-020, in part by the Key Laboratory of Railway Industry of Maglev Technology under Grant TJ202502, in part by the National Railway Administration of P. R. C, in part by the Key Laboratory of Special Machine and High Voltage Apparatus (Shenyang University of Technology), in part by the Ministry of Education under Grant KFKT202403, in part by the State Key Laboratory of Industrial Control Technology through Open Research Project under Grant ICT2025B53, and in part by the National Key Research and Development Program of China under Grant 2024YFB2409200. The work of Jose Rodriguez was supported by ANID under Grant CIA250006. Recommended for publication by Associate Editor H. S. Krishnamoorthy. *(Corresponding author: Lin Qiu.)*

Xing Liu is with the College of Electrical Engineering, Shanghai Dianji University, Shanghai 201306, China, also with the State Key Laboratory of Power Transmission Equipment Technology, School of Electrical Engineering, Chongqing University, Chongqing 401331, China, and also with the College of Electrical Engineering, Zhejiang University, Hangzhou 310027, China (e-mail: xingldl@zju.edu.cn).

Lin Qiu is with the College of Electrical Engineering, Zhejiang University, Hangzhou 310027, China, and also with the Zhejiang University-University of Illinois at Urbana-Champaign Institute, Hangzhou 310027, China (e-mail: qiu_lin@zju.edu.cn).

Youtong Fang is with the College of Electrical Engineering, Zhejiang University, Hangzhou 310027, China (e-mail: youtong@zju.edu.cn).

Kui Wang and Yongdong Li are with the State Key Laboratory of Power System, Department of Electrical Engineering, Tsinghua University, Beijing 100084, China (e-mail: wangkui@tsinghua.edu.cn; liyd@tsinghua.edu.cn).

Jose Rodríguez is with the Faculty of Engineering, Universidad San Sebastian Santiago, Santiago 8420524, Chile (e-mail: jose.rodriguezp@uss.cl).

Color versions of one or more figures in this article are available at https://doi.org/10.1109/TPEL.2025.3642716.

Digital Object Identifier 10.1109/TPEL.2025.3642716

***Index Terms*—Cost function, finite control-set model predictive control (FCS-MPC), low-switching frequency (SF), power converters, reinforcement learning (RL), weighting factors.**

I. Introduction

As A powerful control technology, traditional finite-control set model predictive control (FCS-MPC) is a model-based dynamic optimization approach. In this method, it intends to compute an optimal control input or switching state to drive a dynamical system to a given goal state. In this process, it formulates decision making as an optimization problem, where one evaluates a predefined cost function subject to system's nonlinear constraints stemming from the system dynamics and admissible system states as well as control inputs. The optimization problem is repeatedly solved at each sampling/control instant. The popularity of FCS-MPC is mainly due to its simple and intuitive implementation, the inherent adaptability to power electronic applications, and the ability to cope with multiobjective control problems [1]. Alternatively, the described method provides greater flexibility and more natural formulation. Model-based predictive control design requires, as the name implies, a dynamical model of the controlled process, typically a linear discrete-time one. In the absence of model uncertainty, the problem has been widely studied [2]. With the increase of system complexity in the industrial control applications, some undesired behavior may be caused by the uncertain factors, such as unknown external disturbances, internal parameter uncertainties, and the unnecessary commutation actions of the plant [3], [4]. In that sense, obtaining an accurate plant model becomes computationally demanding and even impossible, evoking significant limitations for implementation. As a consequence, the key issue is how to get rid of this obstacle.

A. Literature Review and Motivation

In the view of feedback, researchers take these barriers into account from different methodologies. It is noteworthy that such a control mechanism should exhibit high adaptability in the face of challenging and adverse scenarios. Due to the increased availability of system data, a possible remedy is to design control solutions such that desired control behavior can be guaranteed by rejecting unknown uncertainties, which is referred to as data-driven predictive control [5], [6]. Specifically, its core idea is to construct a predictive controller directly from measured input/output data of the plant for systems with unknown dynamics, without explicitly identifying a predictive model. This

scheme is not only appealing conceptually but can also be useful in situations where online identification is difficult since it relies on complete system knowledge of the plant. This feature has accelerated the evolution of FCS-MPC solutions. Accordingly, there arises a requirement for a data-driven predictive control capable of offering generalized solutions for power converter applications.

Recently, a data-driven FCS-MPC is proposed in [7], where a model-free adaptive control (MFAC)-based data-driven solution is integrated into the FCS-MPC framework so as to attenuate the sensitiveness to parameter variation and unmodeled dynamics. However, the performance and robustness of data-driven predictive controllers, when the plant is driven by unknown perturbations, are an open concern. For evading this problem, the idea in [7] is further extended by integrating a predictor-based neural network (PNN) into data-driven FCS-MPC framework [8]. Thus, this technique contributes to satisfying performance, while compensating its influence in terms of dealing with unknown disturbances. Although this approach usually results in satisfied performance, controllable switching frequency (SF) are not considered in the design of the controller. This will limit the application of the FCS-MPC scheme in practice. To achieve the accurate control of the SF, a data-driven SF control is embedded into FCS-MPC framework [9], which is partially independent of the plant model and parameter information. Thus, satisfactory SF control behavior can be achieved. Moreover, Huang et al. [10] proposed a codesign of the data-driven predictive voltage control and FCS-MPC for grid-forming inverters under islanded operation, thus facilitating an enhanced voltage regulation performance and system reliability. Despite different successful applications to power electronic control systems have been reported in the literature (see, i.e., [7], [8], [9], and [10]), providing high tracking performance guarantees of data-driven predictive control under parametric uncertainties and measurement noise as well as unknown disturbances remains a widely open research issue.

Following this direction, the FCS-MPC along with online learning technique is another route to circumvent this limitation. The key characteristic behind online learning predictive controllers is to avoid the model parameter identification stage entirely and estimate the model uncertainty and unknown nonlinear dynamics with nonlinear function approximator from artificial intelligence (AI) point of view, e.g., reinforcement learning (RL) [11], recurrent neural network (NN) [12], fuzzy logic system [13], and artificial NN [14]. Among them, online RL deploys natural learning mechanisms and more frequently focuses on performance enhancement by properly modifying their behaviors according to reward and evaluating feedbacks from environments, establishing an optimal control policy to make decisions for various learning tasks. In order to maximize a numerical reward signal, RL is learning how to map situations to actions. Thus, it offers a means for learning agents to interact optimally with uncertain complex environments. Owing to its generalization ability and adaptability to unforeseen scenarios, the RL becomes an ideal choice for controlling power electronic converters [15].

Inspired by this, two novel learning-based predictive control schemes for power converter are, respectively, investigated in [16] and [17], where the offline RL algorithms are leveraged to facilitate weighting factors design and mitigation of model dependence, allowing a superior harmonic performance. However, from a practical point of view, real control environments are typically dynamic, and fixed models based on offline RL often encounter adaptability challenges in new environments due to sample bias. Online RL offers a solution that can update and adjust the model according to changes in the new environment. Especially, further development of online RL technique will enable adaptability and flexibility in dynamic operating conditions. Therefore, it is necessary to design an online learning method with strong adaptability. On account of this idea, Liu et al. [18] developed an online RL predictive control scheme for the power converter systems, which can ensure robust performance under model parameter uncertainty and unknown nonlinear dynamics. Nevertheless, unknown uncertainties under low SF operation may provoke large tracking error. Accordingly, in this background, robust performance under low SF is an important requirement, particularly in medium-voltage high-power applications [19].

As a breakthrough technique, an alternative scheme to addressing SF is inspired by *event-triggered (ET)* point of view along with MPC (ET-MPC) [20]. Only a few articles followed this idea, see the work in [21] considering ET extended state observer (ETESO)-based robust MPC and the work in [22] addressing ETPNN-based MPC for the same purposes as [21]. Specifically, the schemes combine an FCS-MPC protocol with an ET mechanism such that the system uncertainties and unnecessary switching loss are all addressed, eventually resulting in an adequate level of performance. Another recent attempt to avoid the excessive switching losses is presented in [23], where a data-driven controller together with an event-driven idea is designed in order to reduce the average SF and alleviate the sensibility against the parameter variations, thus attenuating the unnecessary commutation actions. Despite the remarkable progress in [18], [19], [20], [21], [22], and [23], the robust control performance under low SF operation is still one key challenge. This barrier triggers additional difficulties to design online learning-based predictive controllers. Consequently, the main motivation of this literature is to simultaneously consider the identified limitations by constructing a data-driven model-free RL FCS-MPC architecture under both unknown uncertainties and low SF scenarios. To facilitate the discussion of various control techniques, the comparison between existing control solutions is provided; see Table I.

B. Main Contribution

Based on the above observations, we are motivated to develop a novel methodology for the aforementioned problems associated with the control performance and challenges in power electronic converter systems. In this article, we further bridge the gap between the classical data-driven predictive control approach and AI technique. Our article aims to better connect these two areas. Specifically, the main idea builds on a proportional-integral (PI)-like data-driven dynamic internal model predictive control (DIMPC) architecture, and integrates the use of variable-step event-driven mechanism and online RL concept for handling

TABLE I
COMPARISON BETWEEN EXISTING CONTROL STRATEGIES

Control methods	Observer-based MFPC [3],[4]	Data-driven -based MFPC [6],[7],[8],[10]	System identification -based FCS-MPC [11],[12],[13],[14]	Model-based ET-MPC [20]	Observer-based ET-MFPC [21],[22]	Offline RL-based MFPC [16],[17]	Data-driven-based model-free RL FCS-MPC
Nature of controller	Nonlinear	Nonlinear	Nonlinear	Nonlinear	Nonlinear	Nonlinear	Nonlinear
Critical design stage	Modulation [3] or Cost Function	Cost Function	Cost Function	Cost function	Cost function	Cost function	Cost function
Robust performance	Excellent	Good	Excellent	Low	Good	Good	Excellent
Control complexity	Moderate	High	High	Moderate	High	High	High
Computational burden	Moderate	High	High	Low	High	High	High
Switching frequency	High	High	High	Moderate	Moderate	High	Low
Tracking performance	Moderate	Moderate	Moderate	Moderate	Moderate	Moderate	Excellent
Antiexternal disturbance	Excellent	Low	Excellent	Low	Excellent	Low	Excellent

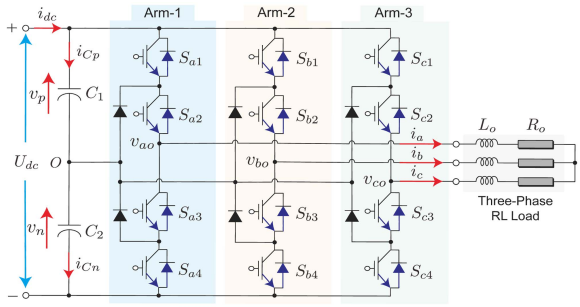

Fig. 1. Circuit topology of three-phase NPC converters.

unknown external disturbances and unnecessary commutation actions. This connection has hitherto remained unexplored in the existing literature. Meanwhile, leveraging this new found connection, our method is capable of yielding valuable insights into the limitations inherent in the existing FCS-MPC for power converter systems, i.e., model parametric uncertainties, uncertain dynamics, unknown disturbances, high SF, unnecessary switching commutation actions, tracking error, and weighting factors. Alternatively, it introduces a design parameter and an error band to determine when to update the RL optimization and maintain the current tracking within the desired limits. More importantly, the primary advantage of our modification is that it allows us to leverage the AI-driven and data-driven as well as event-driven schemes in the context of power converter systems. Details of our proposal are provided in the following sections. Furthermore, the developed control framework is also confirmed by real-world experiments on a power electronic control system with unknown, nonlinear dynamics. Finally, through extensive numerical examples, we illustrate our findings and highlight its merits, and the results demonstrate strong potential to reject model mismatch and unknown disturbances, thus inspiring further investigative work in this area.

II. STANDARD FCS-MPC APPROACH

In this section, we first focus on stating the three-phase three-level neutral-point-clamped (3L-NPC) converters and the FCS-MPC problem, including the discrete-time state-space representation and cost function formulation. Further, the problem statement is also elucidated as follows. The circuit topology of the 3L-NPC converters is shown in Fig. 1.

It consists of three arms, and each inverter arm is composed of four switches and two clamped diodes connected to the neutral point O of a dc bus capacitor. The 3L-NPC converters can produce three switching states in each leg $S_{gx} \in \{-1, 0, 1\}$ and $x \in \{a, b, c\}$. Since the capacitor voltage is equal to a half of the dc-link voltage $U_{\rm dc}$, the converters can produce three voltage levels in each phase, i.e., $v_{xo} = \frac{1}{2}U_{\rm dc}S_{gx}$. The dc-link voltage $U_{\rm dc}$ is divided into $v_p = v_n = U_{\rm dc}/2$, where v_p and v_n denote the dc-link voltages on the high and low sides, respectively. Here, i_a, i_b, and i_c denote three-phase output currents. v_{ao}, v_{bo}, and v_{co} denote three-phase output voltages generated by the converters. C_1 and C_2 denote the dc-link capacitors, respectively. i_{Cp} and i_{Cn} denote the current flowing through each dc-link capacitor. R_o and L_o denote the load resistance and inductance, respectively.

Before moving to the main results, the output voltage and current vectors in the stationary $\alpha\beta$ frame can be transformed in the following equivalent form:

$$\begin{bmatrix} v_\alpha \\ v_\beta \end{bmatrix} = \frac{2}{3}\begin{bmatrix} 1 & -\frac{1}{2} & -\frac{1}{2} \\ 0 & \frac{\sqrt{3}}{2} & -\frac{\sqrt{3}}{2} \end{bmatrix}\begin{bmatrix} v_{ao} \\ v_{bo} \\ v_{co} \end{bmatrix} \tag{1}$$

$$\begin{bmatrix} i_\alpha \\ i_\beta \end{bmatrix} = \frac{2}{3}\begin{bmatrix} 1 & -\frac{1}{2} & -\frac{1}{2} \\ 0 & \frac{\sqrt{3}}{2} & -\frac{\sqrt{3}}{2} \end{bmatrix}\begin{bmatrix} i_a \\ i_b \\ i_c \end{bmatrix}. \tag{2}$$

First of all, the dynamic model of the output currents in the stationary orthogonal $\alpha\beta$ reference frame can be formulated by the following form:

$$\underbrace{\frac{d}{dt}\begin{bmatrix} i_\alpha(t) \\ i_\beta(t) \end{bmatrix}}_{\dot{\boldsymbol{x}}(t)} = \underbrace{\begin{bmatrix} -\frac{R_o}{L_o} & 0 \\ 0 & -\frac{R_o}{L_o} \end{bmatrix}}_{\mathbf{A}}\underbrace{\begin{bmatrix} i_\alpha(t) \\ i_\beta(t) \end{bmatrix}}_{\boldsymbol{x}(t)} + \underbrace{\begin{bmatrix} \frac{1}{L_o} & 0 \\ 0 & \frac{1}{L_o} \end{bmatrix}}_{\mathbf{B}}\underbrace{\begin{bmatrix} v_\alpha(t) \\ v_\beta(t) \end{bmatrix}}_{\boldsymbol{u}(t)} \tag{3}$$

which results in the state-space model in a generic form

$$\begin{cases} \dot{\boldsymbol{x}}(t) = \boldsymbol{A}\boldsymbol{x}(t) + \boldsymbol{B}\boldsymbol{u}(t) \\ \boldsymbol{y}(t) = C\boldsymbol{x}(t) \end{cases} \tag{4}$$

where $\boldsymbol{x}(t)$ denotes the system state vector, $\boldsymbol{u}(t)$ denotes the control input vector, and $\boldsymbol{y}(t)$ denotes the system output vector. Meanwhile, $\mathbf{A}$ denotes the system state matrix, $\mathbf{B}$ denotes the input matrix, and $\mathbf{C}$ denotes the output matrix.

To proceed, we consider the system described by a discrete-time state-space representation in the stationary orthogonal $\alpha\beta$ reference frame

$$\begin{cases} \boldsymbol{x}(k+1) = \mathbf{D}\boldsymbol{x}(k) + \mathbf{E}\boldsymbol{u}(k) \\ \boldsymbol{y}(k) = \mathbf{C}\boldsymbol{x}(k) \end{cases} \tag{5}$$

where $\mathbf{D} = e^{\mathbf{A}T_s}$ and $\mathbf{E} = \mathbf{A}^{-1}(\mathbf{D} - \mathbf{I})\mathbf{B}$, $\mathbf{I}$ denotes the unity matrix with dimensions equal to the dimension of matrix $\mathbf{A}$, and T_s denotes the sampling period.

Thus, the predicted output currents can be obtained in the following equivalent form:

$$\begin{cases} i_\alpha(k+1) = (1-\frac{R_o T_s}{L_o}) i_\alpha(k) + \frac{T_s}{L_o} v_\alpha(k) \\ i_\beta(k+1) = (1-\frac{R_o T_s}{L_o}) i_\beta(k) + \frac{T_s}{L_o} v_\beta(k). \end{cases} \tag{6}$$

Similarly, the predicted dc-link capacitor voltages at the next sampling instant yield

$$\begin{cases} v_p(k+1) = v_p(k) + \frac{1}{C_1} i_{Cp}(k) T_s \\ v_n(k+1) = v_n(k) + \frac{1}{C_2} i_{Cn}(k) T_s. \end{cases} \tag{7}$$

After obtaining the predictions, in order to evaluate system performance, the cost function $\mathcal{J}_C$ (predefined optimization criteria) with the involvement of output current and dc-link voltage terms can be formulated by

$$\mathcal{J}_C = \mathcal{J}_{C1} + \mathcal{J}_{C2} + \lambda_{DC} \mathcal{J}_{C3} \tag{8}$$

$$\begin{cases} \mathcal{J}_{C1} = \|i_\alpha^*(k+1) - i_\alpha(k+1)\|_2^2 \\ \mathcal{J}_{C2} = \|i_\beta^*(k+1) - i_\beta(k+1)\|_2^2 \\ \mathcal{J}_{C3} = \|v_p(k+1) - v_n(k+1)\|_2^2 \end{cases} \tag{9}$$

where $i_\alpha^*(k+1) = 4i_\alpha^*(k) - 6i_\alpha^*(k-1) + 4i_\alpha^*(k-2) - i_\alpha^*(k-3)$ and $i_\beta^*(k+1) = 4i_\beta^*(k) - 6i_\beta^*(k-1) + 4i_\beta^*(k-2) - i_\beta^*(k-3)$ denote the predicted output current references. λ_{DC} is the weighting factor for subcost function $\mathcal{J}_{C3}$. Finally, the optimal voltage vector that minimizes (8) with respect to the aforementioned control objectives is applied in the next sampling period. In other words, the idea behind this technique is to find the optimal switching state (among the finite number of possibilities) that minimizes the cost function value at each sampling instant.

Before presenting the proposal, we give the following problem statement.

Problem Statement: FCS-MPC is an optimization-based solution that yields high-performance control for power converter control systems and ensures satisfaction of system nonlinearities and restrictions. It is interesting to remark that, as aforementioned, this study aims to solve the robust predictive control problem despite unknown external disturbances under low SF scenario [24]. Due to the fact that one of the well-known limitations that affects FCS-MPC performance is represented by model parametric uncertainty [25], [26]. To be more precise, the challenge of the issue stems from the need of accurate model information with respect to a predesigned cost function resulting from decision making subject to system's nonlinear constraints stemming from the system dynamics and available system states, which motivates us to carry out this work.

III. Proposed FCS-MPC Solution

Inspired by these preceding limitations, we discuss how to formulate the robust optimization control problem that yields high-performance guarantees in FCS-MPC framework and to elucidate the main ideas of this proposal. In particular, in this literature, we concentrate on investigating a PI-like data-driven DIMPC method including a nominal controller and a compensatory controller as well as a robust approximate optimal tracking controller to address the parameter uncertainty and the external disturbance as well as optimal tracking problem, respectively. Finally, the block diagram of the proposed FCS-MPC solution is given in Fig. 2.

A. PI-Like Data-Driven DIMPC Controller Design

First, the system (5) subject to modeling uncertainties and external disturbances can be reformulated as the general form. We can get

$$\boldsymbol{y}(k+1) = \boldsymbol{f}(\boldsymbol{y}(k), \boldsymbol{u}_d(k)) + \boldsymbol{\Gamma}(k+1) \tag{10}$$

where $\boldsymbol{f}(\cdot)$ is a generalized function representing the actual system. $\boldsymbol{\Gamma}$ is unknown external disturbance, which is bounded as $\|\boldsymbol{\Gamma}\| \leq \bar{\boldsymbol{\Gamma}}$ where $\bar{\boldsymbol{\Gamma}}$ is a positive constant.

As suggested and drafted in [27], based on two assumptions and Theorem 1, it can be formulated as follows:

$$\Delta \boldsymbol{y}(k+1) = \boldsymbol{\Xi}(k) \Delta \boldsymbol{u}_d(k) + \Delta \boldsymbol{\Gamma}(k+1) \tag{11}$$

where $\boldsymbol{\Xi}(k)$ denotes pseudopartial derivative (PPD) matrix $\Delta \boldsymbol{y}(k+1) = \boldsymbol{y}(k+1) - \boldsymbol{y}(k)$, $\Delta \boldsymbol{u}_d(k) = \boldsymbol{u}_d(k) - \boldsymbol{u}_d(k-1)$, and $\Delta \boldsymbol{\Gamma}(k+1) = \boldsymbol{\Gamma}(k+1) - \boldsymbol{\Gamma}(k)$.

If there is no external disturbance, then the linear data model of (11) becomes a nominal one. It yields

$$\Delta \boldsymbol{y}(k+1) = \boldsymbol{\Xi}(k) \Delta \boldsymbol{u}_d(k) \tag{12}$$

which results in

$$\boldsymbol{y}(k+1) = \boldsymbol{y}(k) + \boldsymbol{\Xi}(k) \Delta \boldsymbol{u}_d(k) \tag{13}$$

which is regarded as the dynamic internal model of plant (10).

Letting $\hat{\boldsymbol{\Xi}}$ denote the estimation of the unavailable $\boldsymbol{\Xi}(k)$, one has

$$\hat{\boldsymbol{y}}(k+1) = \boldsymbol{y}(k) + \hat{\boldsymbol{\Xi}}(k) \Delta \boldsymbol{u}_d(k). \tag{14}$$

Then, one can rewrite (11) as

$$\boldsymbol{y}(k+1) = \boldsymbol{y}(k) + \hat{\boldsymbol{\Xi}}(k) \Delta \boldsymbol{u}_d(k) + \boldsymbol{\Lambda}(k+1) \tag{15}$$

where $\boldsymbol{\Lambda}(k+1) = (\boldsymbol{\Xi}(k) - \hat{\boldsymbol{\Xi}}(k)) \Delta \boldsymbol{u}_d(k) + \Delta \boldsymbol{\Gamma}(k+1)$ denotes the system uncertainties, including both the parameter estimation uncertainty $(\boldsymbol{\Xi}(k) - \hat{\boldsymbol{\Xi}}(k))$ and the unknown external disturbance $\Delta \boldsymbol{\Gamma}(k+1)$. Moreover, as seen from (14) and (15), $\boldsymbol{\Lambda}(k+1) = \boldsymbol{y}(k+1) - \hat{\boldsymbol{y}}(k+1)$ denotes the difference between the actual output and the estimation of nominal output.

To eliminate the undesired external disturbance, the suggested controller along with a disturbance compensator can be formulated as

$$\Delta \boldsymbol{u}_d(k) = \Delta \boldsymbol{u}_c(k) + \Delta \boldsymbol{u}_s(k) \tag{16}$$

where $\Delta \boldsymbol{u}_c(k) = \boldsymbol{u}_c(k) - \boldsymbol{u}_c(k-1)$ denotes the nominal control input, and $\Delta \boldsymbol{u}_s(k) = \boldsymbol{u}_s(k) - \boldsymbol{u}_s(k-1)$ denotes the compensatory control input.

Then, by substituting (16) into (15), we have

$$\begin{aligned} \boldsymbol{y}(k+1) &= \boldsymbol{y}(k) + \hat{\boldsymbol{\Xi}}(k)(\Delta \boldsymbol{u}_c(k) + \Delta \boldsymbol{u}_s(k)) + \boldsymbol{\Lambda}(k+1) \\ &= \boldsymbol{y}(k) + \hat{\boldsymbol{\Xi}}(k) \Delta \boldsymbol{u}_c(k) + \hat{\boldsymbol{\Xi}}(k) \Delta \boldsymbol{u}_s(k) + \boldsymbol{\Lambda}(k+1). \end{aligned} \tag{17}$$

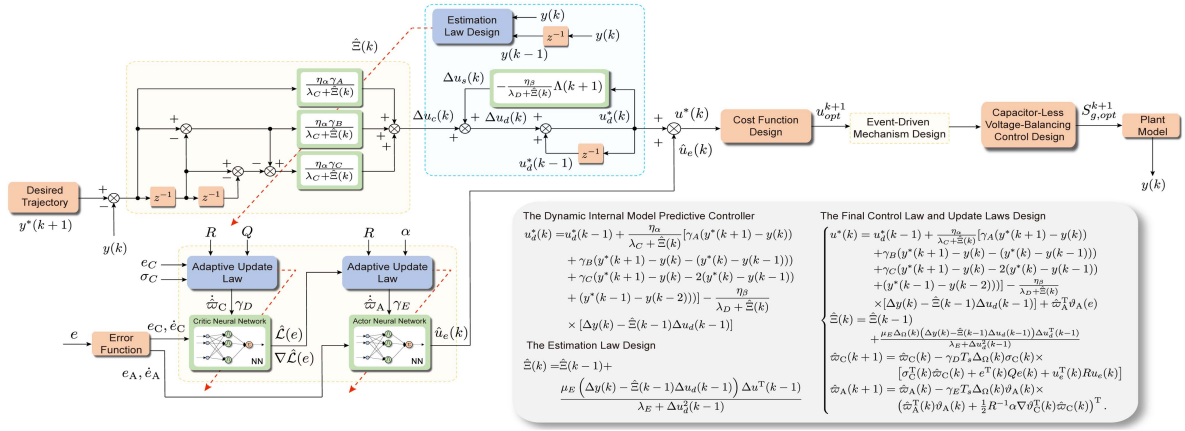

Fig. 2. System configuration and control structure of the proposed FCS-MPC methodology.

We note that to achieve the satisfactory control behavior, a nominal controller is designed, which enables a desired reference trajectory tracking, i.e., $\boldsymbol{y}^*(k+1)=\boldsymbol{y}(k+1)$, and a compensatory controller, which is responsible for rejecting the system uncertainties and unknown disturbances, is introduced into the control design. In order to build it, there exists

$$\begin{cases}\boldsymbol{y}^*(k+1)=\boldsymbol{y}(k)+\hat{\boldsymbol{\Xi}}(k)\Delta\boldsymbol{u}_c(k)\\ 0=\hat{\boldsymbol{\Xi}}(k)\Delta\boldsymbol{u}_s(k)+\boldsymbol{\Lambda}(k+1).\end{cases}\tag{18}$$

On account of the equivalence principle, from (18), it yields

$$\begin{cases}\Delta\boldsymbol{u}_c(k)=\frac{\eta_\alpha}{\lambda_C+\hat{\boldsymbol{\Xi}}(k)}(\boldsymbol{y}^*(k+1)-\boldsymbol{y}(k))\\ \Delta\boldsymbol{u}_s(k)=-\frac{\eta_\beta}{\lambda_D+\hat{\boldsymbol{\Xi}}(k)}\boldsymbol{\Lambda}(k+1)\end{cases}\tag{19}$$

where $\boldsymbol{y}^*(k+1)$ represents a bounded reference output, $\eta_\alpha,\eta_\beta>0$ are two control gains, and, $\lambda_C,\lambda_D>0$ are two small constants. Note that λ_C and λ_D are designed to ensure that the denominator is not equal to zero.

Remark 1: Notice that under low SF operation scenario, unknown parametric uncertainties may result in a larger tracking error that poses a limitation on our control design. To circumvent this issue, a PI-like-based data-driven DIMPC controller is proposed. By combining our innovative technique with existing methods for power converter systems, our development, unlike previous works in the literature [20], [21], [22], contributes to better attenuate capability of parametric uncertainties and high tracking errors.

To enhance the algorithm's generality and robustness, the nominal controller is modified as

$$\begin{aligned}\Delta\boldsymbol{u}_c(k)=&\frac{\eta_\alpha}{\lambda_C+\hat{\boldsymbol{\Xi}}(k)}[\gamma_A(\boldsymbol{y}^*(k+1)-\boldsymbol{y}(k))\\&+\gamma_B(\boldsymbol{y}^*(k+1)-\boldsymbol{y}(k)-(\boldsymbol{y}^*(k)-\boldsymbol{y}(k-1)))\\&+\gamma_C(\boldsymbol{y}^*(k+1)-\boldsymbol{y}(k)-2(\boldsymbol{y}^*(k)-\boldsymbol{y}(k-1))\\&+(\boldsymbol{y}^*(k-1)-\boldsymbol{y}(k-2)))]\end{aligned}\tag{20}$$

where γ_A, γ_B, and γ_C are adjustable parameters to make the proposed control algorithm more flexible.

Remark 2: It can be clearly appreciated that the structure of $\Delta\boldsymbol{u}_c(k)$ in (20) is similar to PI control. Thus, the control parameters can be selected based on the experience of PI control. The key distinction between PI control and PI-like data-driven DIMPC is that the parameter of $\Delta\boldsymbol{u}_d(k)$ is adaptive due to $\boldsymbol{\Xi}(k)$, which facilitates performance enhancement.

Since $\boldsymbol{\Xi}(k)$ is unknown, the projection algorithm is here deployed to estimate the unknown PPD with the following objective function:

$$\mathcal{J}_E(\hat{\boldsymbol{\Xi}}(k))=\mathcal{J}_{E1}+\lambda_E\mathcal{J}_{E2}\tag{21}$$

$$\begin{cases}\mathcal{J}_{E1}=|\Delta\boldsymbol{y}(k)-\hat{\boldsymbol{\Xi}}(k)\Delta\boldsymbol{u}_d(k-1)|^2\\ \mathcal{J}_{E2}=|\hat{\boldsymbol{\Xi}}(k)-\hat{\boldsymbol{\Xi}}(k-1)|^2\end{cases}\tag{22}$$

where $\lambda_E>0$ is a weighting factor.

Thus, minimize the objective function (21) with respect to $\boldsymbol{\Xi}(k)$ and introduce the estimation law as

$$\begin{aligned}\hat{\boldsymbol{\Xi}}(k)=&\hat{\boldsymbol{\Xi}}(k-1)\\&+\frac{\mu_E\left(\Delta\boldsymbol{y}(k)-\hat{\boldsymbol{\Xi}}(k-1)\Delta\boldsymbol{u}_d(k-1)\right)\Delta\boldsymbol{u}^{\mathrm{T}}(k-1)}{\lambda_E+\Delta\boldsymbol{u}_d^2(k-1)}\end{aligned}\tag{23}$$

where $\mu_E>0$ is a step factor and $\hat{\boldsymbol{\Xi}}(k)$ is the estimation of $\boldsymbol{\Xi}(k)$.

On the other hand, if the sampling period T_s is assumed to be small, then the parameter estimation and external disturbances signals are assumed to be constant over the switching period $\boldsymbol{\Lambda}(k+1)\approx\boldsymbol{\Lambda}(k)$. This is reasonable, in practical applications, since a power converter control system cannot realistically handle arbitrarily fast external signals in one sampling period T_s. Thus, the compensatory controller $\Delta\boldsymbol{u}_s(k)$ in (19) can be obtained in the following equivalent form:

$$\begin{aligned}\Delta\boldsymbol{u}_s(k)&=-\frac{\eta_\beta}{\lambda_D+\hat{\boldsymbol{\Xi}}(k)}[\Delta\boldsymbol{y}(k+1)-\hat{\boldsymbol{\Xi}}(k)\Delta\boldsymbol{u}_d(k)]\\&=-\frac{\eta_\beta}{\lambda_D+\hat{\boldsymbol{\Xi}}(k)}[\Delta\boldsymbol{y}(k)-\hat{\boldsymbol{\Xi}}(k-1)\Delta\boldsymbol{u}_d(k-1)].\end{aligned}\tag{24}$$

Based on the above representation, the developed controller and the estimation law are established as

$$\begin{cases}\Delta \boldsymbol{u}_c(k) = \frac{\eta_\alpha}{\lambda_C+\hat{\boldsymbol{\Xi}}(k)}[\gamma_A(\boldsymbol{y}^*(k+1)-\boldsymbol{y}(k)) \\ \quad +\gamma_B(\boldsymbol{y}^*(k+1)-\boldsymbol{y}(k)-(\boldsymbol{y}^*(k)-\boldsymbol{y}(k-1))) \\ \quad +\gamma_C(\boldsymbol{y}^*(k+1)-\boldsymbol{y}(k)-2(\boldsymbol{y}^*(k)-\boldsymbol{y}(k-1)) \\ \quad +(\boldsymbol{y}^*(k-1)-\boldsymbol{y}(k-2)))] \\ \Delta \boldsymbol{u}_s(k) = -\frac{\eta_\beta}{\lambda_D+\hat{\boldsymbol{\Xi}}(k)}[\Delta \boldsymbol{y}(k)-\hat{\boldsymbol{\Xi}}(k-1)\Delta \boldsymbol{u}_d(k-1)] \\ \hat{\boldsymbol{\Xi}}(k) = \hat{\boldsymbol{\Xi}}(k-1)+\frac{\mu_E\left(\Delta \boldsymbol{y}(k)-\hat{\boldsymbol{\Xi}}(k-1)\Delta \boldsymbol{u}_d(k-1)\right)\Delta \boldsymbol{u}_d^{\mathrm{T}}(k-1)}{\lambda_E+\Delta \boldsymbol{u}_d^2(k-1)}.\end{cases} \tag{25}$$

Then, the control law in (16) can be transformed as

$$\begin{aligned}\Delta \boldsymbol{u}_d(k) &= \Delta \boldsymbol{u}_c(k)+\Delta \boldsymbol{u}_s(k) \\ &= \frac{\eta_\alpha}{\lambda_C+\hat{\boldsymbol{\Xi}}(k)}[\gamma_A(\boldsymbol{y}^*(k+1)-\boldsymbol{y}(k)) \\ &\quad +\gamma_B(\boldsymbol{y}^*(k+1)-\boldsymbol{y}(k)-(\boldsymbol{y}^*(k)-\boldsymbol{y}(k-1))) \\ &\quad +\gamma_C(\boldsymbol{y}^*(k+1)-\boldsymbol{y}(k)-2(\boldsymbol{y}^*(k)-\boldsymbol{y}(k-1)) \\ &\quad +(\boldsymbol{y}^*(k-1)-\boldsymbol{y}(k-2)))]-\frac{\eta_\beta}{\lambda_D+\hat{\boldsymbol{\Xi}}(k)} \\ &\quad \times[\Delta \boldsymbol{y}(k)-\hat{\boldsymbol{\Xi}}(k-1)\Delta \boldsymbol{u}_d(k-1)].\end{aligned} \tag{26}$$

Finally, the developed DIMPC controller and the estimation law can be reconstructed by

$$\begin{cases}\boldsymbol{u}_d^*(k) = \boldsymbol{u}_d^*(k-1)+\frac{\eta_\alpha}{\lambda_C+\hat{\boldsymbol{\Xi}}(k)}[\gamma_A(\boldsymbol{y}^*(k+1)-\boldsymbol{y}(k)) \\ \quad +\gamma_B(\boldsymbol{y}^*(k+1)-\boldsymbol{y}(k)-(\boldsymbol{y}^*(k)-\boldsymbol{y}(k-1))) \\ \quad +\gamma_C(\boldsymbol{y}^*(k+1)-\boldsymbol{y}(k)-2(\boldsymbol{y}^*(k)-\boldsymbol{y}(k-1)) \\ \quad +(\boldsymbol{y}^*(k-1)-\boldsymbol{y}(k-2)))]-\frac{\eta_\beta}{\lambda_D+\hat{\boldsymbol{\Xi}}(k)} \\ \quad \times[\Delta \boldsymbol{y}(k)-\hat{\boldsymbol{\Xi}}(k-1)\Delta \boldsymbol{u}_d(k-1)] \\ \hat{\boldsymbol{\Xi}}(k) = \hat{\boldsymbol{\Xi}}(k-1)+\frac{\mu_E\left(\Delta \boldsymbol{y}(k)-\hat{\boldsymbol{\Xi}}(k-1)\Delta \boldsymbol{u}_d(k-1)\right)\Delta \boldsymbol{u}_d^{\mathrm{T}}(k-1)}{\lambda_E+\Delta \boldsymbol{u}_d^2(k-1)}.\end{cases} \tag{27}$$

Remark 3: Note that the developed DIMPC controller can achieve the control aim without necessarily leveraging or needing a model of the plant. Although this proposal has brought some improvements, little research has been focused on trying to incorporate an RL technique into a data-driven DIMPC framework in an optimal manner. Accordingly, it is expected to simultaneously address the unnecessary switching commutation actions, tracking error, and unknown uncertainties in FCS-MPC for power converters, without weighting factors. In the following, the establishment of RL-based robust approximate optimal tracking controller design is discussed in detail.

B. RL-Based Robust Approximate Optimal Tracking Controller Design

In the following, in order to address the optimal tracking control issue and stabilize the tracking error dynamics in an optimal manner, a feedback controller $\boldsymbol{u}_e$ will be designed. First, the following performance index can defined as [28]:

$$\mathcal{L}(\boldsymbol{e}) = \int_t^\infty r(\boldsymbol{e}(\tau), \boldsymbol{u}_e(\tau))d\tau \tag{28}$$

where $r(\boldsymbol{e}, \boldsymbol{u}_e) = \boldsymbol{e}^{\mathrm{T}}Q\boldsymbol{e}+\boldsymbol{u}_e^{\mathrm{T}}R\boldsymbol{u}_e$ is the utility function, and Q and R are symmetric positive-definite matrices with appropriate dimensions, $\boldsymbol{u}_e = \boldsymbol{u}-\boldsymbol{u}_d^*$, and $\boldsymbol{e} = \boldsymbol{x}-\boldsymbol{x}_d$. $\boldsymbol{x}_d$ denotes the desired trajectory.

Second, we recall the dynamic model (4), and then, the system with modeling uncertainties and external disturbances can be reformulated into the ultralocal model form

$$\dot{\boldsymbol{x}} = \boldsymbol{f}+\boldsymbol{\alpha}\boldsymbol{u} \tag{29}$$

where $\boldsymbol{f} = \mathbf{A}\boldsymbol{x}+\boldsymbol{\Gamma}$ is the lumped uncertainty, which includes system uncertainties and the external disturbance assumed to be bounded, and $\boldsymbol{\alpha}$ is a nonzero nonphysical constant denoting the control input gain.

Based on the tracking error $\boldsymbol{e} = \boldsymbol{x}-\boldsymbol{x}_d$, the error system can be represented by the following form:

$$\dot{\boldsymbol{e}} = \dot{\boldsymbol{x}}-\dot{\boldsymbol{x}}_d = \boldsymbol{f}_e+\boldsymbol{\alpha}\boldsymbol{u}_e \tag{30}$$

where $\boldsymbol{f}_e = \boldsymbol{f}(\boldsymbol{x})-\boldsymbol{f}(\boldsymbol{x}_d)$. Note that the controller $\boldsymbol{u}$ is composed of two parts, i.e., the suggested steady-state controller $\boldsymbol{u}_d^*$, and the feedback controller $\boldsymbol{u}_e$. To be more precise, the proposed control scheme combines a PI-like data-driven DIMPC controller and an approximate optimal controller.

Next, we formulate the Hamiltonian function as

$$H(\boldsymbol{e}, \boldsymbol{u}_e, \nabla\mathcal{L}(\boldsymbol{e})) = \nabla\mathcal{L}^{\mathrm{T}}(\boldsymbol{f}_e+\boldsymbol{\alpha}\boldsymbol{u}_e)+\boldsymbol{e}^{\mathrm{T}}Q\boldsymbol{e}+\boldsymbol{u}_e^{\mathrm{T}}R\boldsymbol{u}_e \tag{31}$$

where $\nabla\mathcal{L}(\boldsymbol{e}) = \partial\mathcal{L}(\boldsymbol{e})/\partial\boldsymbol{e}$ is the partial derivative of the cost function $\mathcal{L}(\boldsymbol{e})$ with respect to $\boldsymbol{e}$.

The optimal performance index $\mathcal{L}^*(\boldsymbol{e})$ is defined as

$$\mathcal{L}^*(\boldsymbol{e}) = \min_{\boldsymbol{u}_e\in\Psi(\Omega)}\left(\int_t^\infty r(\boldsymbol{e}(\tau), \boldsymbol{u}_e(\tau))d\tau\right) \tag{32}$$

and satisfies

$$0 = \min_{\boldsymbol{u}_e\in\Psi(\Omega)}[H(\boldsymbol{e}, \boldsymbol{u}_e, \nabla\mathcal{L}^*(\boldsymbol{e}))]. \tag{33}$$

In addition, we can obtain the optimal control policy $\boldsymbol{u}_e^*$ by solving $\partial H(\boldsymbol{e}, \boldsymbol{u}_e, \nabla\mathcal{L}^*(\boldsymbol{e}))/\partial\boldsymbol{u}_e = 0$ as

$$\boldsymbol{u}_e^* = -\frac{1}{2}R^{-1}\boldsymbol{\alpha}\nabla\mathcal{L}^*(\boldsymbol{e}) \tag{34}$$

where $\nabla\mathcal{L}^*(\boldsymbol{e}) = \partial\mathcal{L}^*(\boldsymbol{e})/\partial\boldsymbol{e}$. Thus, the overall optimal control input can be rewritten as $\boldsymbol{u}^* = \boldsymbol{u}_d^*+\boldsymbol{u}_e^*$.

Remark 4: Notably, the Hamilton-Jacobi-Bellman (HJB) equation in (33) is a nonlinear partial differential equation that is highly challenging to solve owing to its inherent nonlinearity. Accordingly, in what follows, we will focus on designing an optimal feedback controller via the adaptive dynamic programming (ADP) method, which is realized by utilizing critic and actor NNs [29], [30]. It should be emphasized that unlike conventional ADP approaches where critic and actor NN weights are updated sequentially, the weights of both critic and action NNs can be updated in real time simultaneously, enabling synchronous online implementation.

C. Critic NN Design

According to the prominent approximation capability of NN, a single hidden layer NN is here deployed to approximate $\mathcal{L}(\boldsymbol{e})$

as

$$\mathcal{L}(\boldsymbol{e}) = \boldsymbol{\varpi}_{\mathrm{C}}^{\mathrm{T}}\boldsymbol{\vartheta}_{\mathrm{C}}(\boldsymbol{e}) + \boldsymbol{\varepsilon}_{\mathrm{C}} \tag{35}$$

where $\boldsymbol{\varpi}_{\mathrm{C}}$ denotes the optimal weight, satisfying $\|\boldsymbol{\varpi}_{\mathrm{C}}\|_{\mathrm{F}} \leq \bar{\boldsymbol{\varpi}}_{\mathrm{C}}$ with $\bar{\boldsymbol{\varpi}}_{\mathrm{C}} \in \Re$ being positive constants, $\boldsymbol{\varepsilon}_{\mathrm{C}}$ denotes the critic NN approximation error, and $\|\boldsymbol{\varepsilon}_{\mathrm{C}}\| \leq \bar{\boldsymbol{\varepsilon}}_{\mathrm{C}}$ with $\bar{\boldsymbol{\varepsilon}}_{\mathrm{C}} \in \Re$ being positive constants.

Then, we can further derive

$$\nabla\mathcal{L}(\boldsymbol{e}) = \nabla\boldsymbol{\vartheta}_{\mathrm{C}}^{\mathrm{T}}\boldsymbol{\varpi}_{\mathrm{C}} + \nabla\boldsymbol{\varepsilon}_{\mathrm{C}} \tag{36}$$

where $\nabla\boldsymbol{\vartheta}_{\mathrm{C}} = \partial\boldsymbol{\vartheta}_{\mathrm{C}}(\boldsymbol{e})/\partial\boldsymbol{e}$ denotes the activation function gradient, and is upper bounded so that $\|\nabla\boldsymbol{\vartheta}_{\mathrm{C}}\| \leq \boldsymbol{\vartheta}_{\mathrm{CM}}$, and $\nabla\boldsymbol{\varepsilon}_{\mathrm{C}} = \partial\boldsymbol{\varepsilon}_{\mathrm{C}}(\boldsymbol{e})/\partial\boldsymbol{e}$ denotes the NN reconstruction error gradient.

Let $\hat{\boldsymbol{\varpi}}_{\mathrm{C}}$ be an estimate of $\boldsymbol{\varpi}_{\mathrm{C}}$, and a critic NN is here utilized to approximate the value function. Then, the estimate of $\mathcal{L}(\boldsymbol{e})$ yields

$$\hat{\mathcal{L}}(\boldsymbol{e}) = \hat{\boldsymbol{\varpi}}_{\mathrm{C}}^{\mathrm{T}}\boldsymbol{\vartheta}_{\mathrm{C}}(\boldsymbol{e}). \tag{37}$$

Leading to the following gradient:

$$\nabla\hat{\mathcal{L}}(\boldsymbol{e}) = (\nabla\boldsymbol{\vartheta}_{\mathrm{C}}(\boldsymbol{e}))^{\mathrm{T}}\hat{\boldsymbol{\varpi}}_{\mathrm{C}} \tag{38}$$

where $\nabla\hat{\mathcal{L}}(\boldsymbol{e}) = \partial\hat{\mathcal{L}}(\boldsymbol{e})/\partial\boldsymbol{e}$.

Next, the approximate Hamiltonian function can be expressed as

$$\begin{aligned} H(\boldsymbol{e}, \boldsymbol{u}_e, \hat{\boldsymbol{\varpi}}_{\mathrm{C}}) &= \nabla\boldsymbol{\vartheta}_{\mathrm{C}}^{\mathrm{T}}\hat{\boldsymbol{\varpi}}_{\mathrm{C}}(\boldsymbol{f}_e + \boldsymbol{\alpha}\boldsymbol{u}_e) + \boldsymbol{e}^{\mathrm{T}}Q\boldsymbol{e} + \boldsymbol{u}_e^{\mathrm{T}}R\boldsymbol{u}_e \\ &= \nabla\boldsymbol{\vartheta}_{\mathrm{C}}^{\mathrm{T}}\hat{\boldsymbol{\varpi}}_{\mathrm{C}}\left\{[\boldsymbol{f}(\boldsymbol{x}) - \boldsymbol{f}(\boldsymbol{x}_d)] + \boldsymbol{\alpha}\boldsymbol{u}_e + \boldsymbol{\varepsilon}_e\right\} \\ &= \nabla\boldsymbol{\vartheta}_{\mathrm{C}}^{\mathrm{T}}\hat{\boldsymbol{\varpi}}_{\mathrm{C}}\left\{\hat{\boldsymbol{\varpi}}_{\mathrm{B}}[\boldsymbol{\vartheta}_{\mathrm{B}}^{\mathrm{T}}(\boldsymbol{x}) - \boldsymbol{\vartheta}_{\mathrm{B}}^{\mathrm{T}}(\boldsymbol{x}_d)] + \boldsymbol{\alpha}\boldsymbol{u}_e\right. \\ &\quad \left.+\boldsymbol{\varepsilon}_e\right\} + \boldsymbol{e}^{\mathrm{T}}Q\boldsymbol{e} + \boldsymbol{u}_e^{\mathrm{T}}R\boldsymbol{u}_e = \boldsymbol{e}_{\mathrm{C}} \end{aligned} \tag{39}$$

where $\boldsymbol{\varepsilon}_e$ represents the total residual error, satisfying $\|\boldsymbol{\varepsilon}_e\| \leq \bar{\boldsymbol{\varepsilon}}_e$ with $\bar{\boldsymbol{\varepsilon}}_e \in \Re$ being positive constants. Due to the ability of NNs to approximate a given continuous nonlinear function, we can get $\boldsymbol{f}(\boldsymbol{x}) = \boldsymbol{\varpi}_{\mathrm{B}}^{\mathrm{T}}\boldsymbol{\vartheta}_{\mathrm{B}}(\boldsymbol{x}) + \boldsymbol{\varepsilon}_{\mathrm{B}}$, where $\boldsymbol{\varpi}_{\mathrm{B}}$ denotes the optimal weight matrix subject to $\|\boldsymbol{\varpi}_{\mathrm{B}}\|_{\mathrm{F}} \leq \bar{\boldsymbol{\varpi}}_{\mathrm{B}}$ with $\bar{\boldsymbol{\varpi}}_{\mathrm{B}} \in \Re$ being positive constants. Here, $\boldsymbol{\varepsilon}_{\mathrm{B}}$ denotes the minimum approximation error, satisfying $\|\boldsymbol{\varepsilon}_{\mathrm{B}}\| \leq \bar{\boldsymbol{\varepsilon}}_{\mathrm{B}}$ with $\bar{\boldsymbol{\varepsilon}}_{\mathrm{B}} \in \Re$ being positive constants.

To design an update law for $\hat{\boldsymbol{\varpi}}_{\mathrm{B}}$, a state predictor is utilized herein by the following form [22]:

$$\begin{cases} \dot{\hat{\boldsymbol{x}}} = \hat{\boldsymbol{\varpi}}_{\mathrm{B}}^{\mathrm{T}}\boldsymbol{\vartheta}_{\mathrm{B}}(\boldsymbol{x}) + \boldsymbol{\alpha}\boldsymbol{u} - k_1\tilde{\boldsymbol{x}} \\ \dot{\hat{\boldsymbol{\varpi}}}_{\mathrm{B}} = -\Gamma_{\mathrm{B}}[\boldsymbol{\vartheta}_{\mathrm{B}}(\boldsymbol{x})\tilde{\boldsymbol{x}} + k_{w1}\hat{\boldsymbol{\varpi}}_{\mathrm{B}}] \end{cases} \tag{40}$$

where $k_1 \in \Re$, $\Gamma_{\mathrm{B}} \in \Re$, and $k_{w1} \in \Re$ are positive constants, respectively, and $\tilde{\boldsymbol{x}} = \hat{\boldsymbol{x}} - \boldsymbol{x}$. $\hat{\boldsymbol{x}}$ denotes the observed value of $\boldsymbol{x}$.

We note that it is desired to select $\hat{\boldsymbol{\varpi}}_{\mathrm{C}}$ to minimize the squared residual error $\mathrm{E}_{\mathrm{C}}(\hat{\boldsymbol{\varpi}}_{\mathrm{C}})$ as

$$\mathrm{E}_{\mathrm{C}}(\hat{\boldsymbol{\varpi}}_{\mathrm{C}}) = \frac{1}{2}\boldsymbol{e}_{\mathrm{C}}^{\mathrm{T}}\boldsymbol{e}_{\mathrm{C}}. \tag{41}$$

For implementation, the critic NN weight update law can be represented

$$\begin{aligned} \dot{\hat{\boldsymbol{\varpi}}}_{\mathrm{C}} &= -\gamma_D\frac{\partial\mathrm{E}_{\mathrm{C}}}{\partial\hat{\boldsymbol{\varpi}}_{\mathrm{C}}} \\ &= -\gamma_D\boldsymbol{\sigma}_{\mathrm{C}}\left(\boldsymbol{\sigma}_{\mathrm{C}}^{\mathrm{T}}\hat{\boldsymbol{\varpi}}_{\mathrm{C}} + \boldsymbol{e}^{\mathrm{T}}Q\boldsymbol{e} + \boldsymbol{u}_e^{\mathrm{T}}R\boldsymbol{u}_e\right) \end{aligned} \tag{42}$$

where $\gamma_D > 0$ is the critic NN learning rate, $\boldsymbol{\sigma}_{\mathrm{C}} = \boldsymbol{\sigma}/(\boldsymbol{\sigma}^{\mathrm{T}}\boldsymbol{\sigma} + 1)$, and $\boldsymbol{\sigma} = \nabla\boldsymbol{\vartheta}_{\mathrm{C}}^{\mathrm{T}}[\hat{\boldsymbol{\varpi}}_{\mathrm{B}}(\boldsymbol{\vartheta}_{\mathrm{B}}^{\mathrm{T}}(\boldsymbol{x}) - \boldsymbol{\vartheta}_{\mathrm{B}}^{\mathrm{T}}(\boldsymbol{x}_d)) + \boldsymbol{\alpha}\boldsymbol{u}_e + \boldsymbol{\varepsilon}_e] = \nabla\boldsymbol{\vartheta}_{\mathrm{C}}^{\mathrm{T}}[\boldsymbol{f}_e + \boldsymbol{\alpha}\boldsymbol{u}_e]$. According to the definition of $\boldsymbol{\sigma}_{\mathrm{C}}$, there exists a positive constant $\boldsymbol{\sigma}_{\mathrm{CM}} > 1$ such that $\|\boldsymbol{\sigma}_{\mathrm{C}}\| \leq \boldsymbol{\sigma}_{\mathrm{CM}}$.

D. Actor NN Design

Similarly, the policy of the feedback control can be approximated by the actor NN as

$$\boldsymbol{u}_e = \boldsymbol{\varpi}_{\mathrm{A}}^{\mathrm{T}}\boldsymbol{\vartheta}_{\mathrm{A}}(\boldsymbol{e}) + \boldsymbol{\varepsilon}_{\mathrm{A}} \tag{43}$$

where $\boldsymbol{\varpi}_{\mathrm{A}}$ denotes the optimal weight, satisfying $\|\boldsymbol{\varpi}_{\mathrm{A}}\|_{\mathrm{F}} \leq \bar{\boldsymbol{\varpi}}_{\mathrm{A}}$ with $\bar{\boldsymbol{\varpi}}_{\mathrm{A}} \in \Re$ being positive constants, $\boldsymbol{\varepsilon}_{\mathrm{A}}$ denotes the actor NN approximation error, and $\|\boldsymbol{\varepsilon}_{\mathrm{A}}\| \leq \bar{\boldsymbol{\varepsilon}}_{\mathrm{A}}$ with $\bar{\boldsymbol{\varepsilon}}_{\mathrm{A}} \in \Re$ being positive constants. The vector of the activation function of the actor NN, i.e., $\boldsymbol{\vartheta}_{\mathrm{A}}$, is upper bounded so that $\|\boldsymbol{\vartheta}_{\mathrm{A}}(\cdot)\| \leq \boldsymbol{\vartheta}_{\mathrm{AM}}$.

Let $\hat{\boldsymbol{\varpi}}_{\mathrm{A}}$ be an estimate of $\boldsymbol{\varpi}_{\mathrm{A}}$, then the approximated optimal feedback control policy can be expressed as

$$\hat{\boldsymbol{u}}_e = \hat{\boldsymbol{\varpi}}_{\mathrm{A}}^{\mathrm{T}}\boldsymbol{\vartheta}_{\mathrm{A}}(\boldsymbol{e}). \tag{44}$$

The tuning of the actor NN can be achieved by utilizing the feedback error signal, which serves to represent the difference between the feedback control input applied to the error system (30) and the control input that minimizes (37). Thus, one has

$$\boldsymbol{e}_{\mathrm{A}} = \hat{\boldsymbol{\varpi}}_{\mathrm{A}}^{\mathrm{T}}\boldsymbol{\vartheta}_{\mathrm{A}} + \frac{1}{2}R^{-1}\boldsymbol{\alpha}\nabla\boldsymbol{\vartheta}_{\mathrm{C}}^{\mathrm{T}}\hat{\boldsymbol{\varpi}}_{\mathrm{C}}. \tag{45}$$

The objective function can be minimized through the actor NN, and so we get

$$\mathrm{E}_{\mathrm{A}}(\hat{\boldsymbol{\varpi}}_{\mathrm{A}}) = \frac{1}{2}\boldsymbol{e}_{\mathrm{A}}^{\mathrm{T}}\boldsymbol{e}_{\mathrm{A}}. \tag{46}$$

Thus, the actor NN weight update law yields

$$\dot{\hat{\boldsymbol{\varpi}}}_{\mathrm{A}} = -\gamma_E\boldsymbol{\vartheta}_{\mathrm{A}}\left(\hat{\boldsymbol{\varpi}}_{\mathrm{A}}^{\mathrm{T}}\boldsymbol{\vartheta}_{\mathrm{A}} + \frac{1}{2}R^{-1}\boldsymbol{\alpha}\nabla\boldsymbol{\vartheta}_{\mathrm{C}}^{\mathrm{T}}\hat{\boldsymbol{\varpi}}_{\mathrm{C}}\right)^{\mathrm{T}} \tag{47}$$

where $\gamma_E > 0$ is the actor NN learning rate.

Then, the final optimal control input can be obtained

$$\boldsymbol{u}^* = \boldsymbol{u}_d^* + \hat{\boldsymbol{u}}_e \tag{48}$$

which results in

$$\begin{cases} \boldsymbol{u}^*(k) = \boldsymbol{u}_d^*(k-1) + \frac{\eta_\alpha}{\lambda_C + \hat{\boldsymbol{\Xi}}(k)}[\gamma_A(\boldsymbol{y}^*(k+1) - \boldsymbol{y}(k)) \\ \qquad + \gamma_B(\boldsymbol{y}^*(k+1) - \boldsymbol{y}(k) - (\boldsymbol{y}^*(k) - \boldsymbol{y}(k-1))) \\ \qquad + \gamma_C(\boldsymbol{y}^*(k+1) - \boldsymbol{y}(k) - 2(\boldsymbol{y}^*(k) - \boldsymbol{y}(k-1)) \\ \qquad + (\boldsymbol{y}^*(k-1) - \boldsymbol{y}(k-2)))] - \frac{\eta_\beta}{\lambda_D + \hat{\boldsymbol{\Xi}}(k)} \\ \qquad \times [\Delta\boldsymbol{y}(k) - \hat{\boldsymbol{\Xi}}(k-1)\Delta\boldsymbol{u}_d(k-1)] + \hat{\boldsymbol{\varpi}}_{\mathrm{A}}^{\mathrm{T}}\boldsymbol{\vartheta}_{\mathrm{A}}(\boldsymbol{e}) \\ \hat{\boldsymbol{\Xi}}(k) = \hat{\boldsymbol{\Xi}}(k-1) + \frac{\mu_E\left(\Delta\boldsymbol{y}(k) - \hat{\boldsymbol{\Xi}}(k-1)\Delta\boldsymbol{u}_d(k-1)\right)\Delta\boldsymbol{u}_d^{\mathrm{T}}(k-1)}{\lambda_E + \Delta\boldsymbol{u}_d^2(k-1)} \\ \hat{\boldsymbol{\varpi}}_{\mathrm{C}}(k+1) = \hat{\boldsymbol{\varpi}}_{\mathrm{C}}(k) - \gamma_D T_s\boldsymbol{\sigma}_{\mathrm{C}}(k)\times \\ \qquad \left[\boldsymbol{\sigma}_{\mathrm{C}}^{\mathrm{T}}(k)\hat{\boldsymbol{\varpi}}_{\mathrm{C}}(k) + \boldsymbol{e}^{\mathrm{T}}(k)Q\boldsymbol{e}(k) + \boldsymbol{u}_e^{\mathrm{T}}(k)R\boldsymbol{u}_e(k)\right] \\ \hat{\boldsymbol{\varpi}}_{\mathrm{A}}(k+1) = \hat{\boldsymbol{\varpi}}_{\mathrm{A}}(k) - \gamma_E T_s\boldsymbol{\vartheta}_{\mathrm{A}}(k)\times \\ \qquad \left(\hat{\boldsymbol{\varpi}}_{\mathrm{A}}^{\mathrm{T}}(k)\boldsymbol{\vartheta}_{\mathrm{A}}(k) + \frac{1}{2}R^{-1}\boldsymbol{\alpha}\nabla\boldsymbol{\vartheta}_{\mathrm{C}}^{\mathrm{T}}(k)\hat{\boldsymbol{\varpi}}_{\mathrm{C}}(k)\right)^{\mathrm{T}}. \end{cases} \tag{49}$$

E. Design of Cost Function

In general, the cost function is constructed according to the user-predefined control objectives. In this article, to avoid this challenge caused by the cumbersome tuning of weighting factors, one seeks to regulate the system control input to desired reference without weighting factors. Based on the detailed analysis above, the cost function for the output voltage tracking can be designed as

$$\mathcal{J}_F = \|\boldsymbol{u}^*(k+1) - \boldsymbol{u}(k+1)\|_2^2. \tag{50}$$

Remark 5: It is worth noting that although the above presented studies make significant advances, the high SF is still open and challenging to be investigated in the control problem formulation. To solve this issue, a low SF data-driven DIMPC framework that alleviates the unnecessary switching commutation actions by leveraging a variable-step event-driven mechanism point of view is developed in this literature.

F. Variable-Step Event-Driven Mechanism Design

As demonstrated above, due to the inevitable uncertainties in practical systems, false events may be generated, and thus leading to some unnecessary triggering [21], [22]. To circumvent this obstacle, in this section, we further exploit a variable-step event-driven MFPC framework [23]. Following [23], the event-driven conditions together with a user-predesigned threshold δ_e are given to judge if $\boldsymbol{u}(k)$ and the weight update laws can be maintained. Then, the modified weight update laws are reconstructed by the following expression:

$$\boldsymbol{u}^{\text{opt}}(k+1) = \begin{cases} \boldsymbol{u}(k), \ \text{if} |\boldsymbol{e}(k+1)| \le \delta_e^2 \Rightarrow \Delta_\Omega(k) = 0 \\ \min \mathcal{J}_F, \text{if} |\boldsymbol{e}(k+1)| > \delta_e^2 \Rightarrow \Delta_\Omega(k) = 1 \end{cases} \tag{51}$$

$$\begin{cases} \hat{\boldsymbol{\Xi}}(k) = \hat{\boldsymbol{\Xi}}(k-1) \\ \qquad + \frac{\mu_E \Delta_\Omega(k)\left(\Delta \boldsymbol{y}(k) - \hat{\boldsymbol{\Xi}}(k-1)\Delta \boldsymbol{u}_d(k-1)\right)\Delta \boldsymbol{u}_d^{\mathrm{T}}(k-1)}{\lambda_E + \Delta \boldsymbol{u}_d^2(k-1)} \\ \hat{\boldsymbol{\varpi}}_{\mathrm{C}}(k+1) = \hat{\boldsymbol{\varpi}}_{\mathrm{C}}(k) - \gamma_D T_s \Delta_\Omega(k) \boldsymbol{\sigma}_{\mathrm{C}}(k) \times \\ \qquad \left[\boldsymbol{\sigma}_{\mathrm{C}}^{\mathrm{T}}(k)\hat{\boldsymbol{\varpi}}_{\mathrm{C}}(k) + \boldsymbol{e}^{\mathrm{T}}(k) Q \boldsymbol{e}(k) + \boldsymbol{u}_e^{\mathrm{T}}(k) R \boldsymbol{u}_e(k)\right] \\ \hat{\boldsymbol{\varpi}}_{\mathrm{A}}(k+1) = \hat{\boldsymbol{\varpi}}_{\mathrm{A}}(k) - \gamma_E T_s \Delta_\Omega(k) \boldsymbol{\vartheta}_{\mathrm{A}}(k) \times \\ \qquad \left(\hat{\boldsymbol{\varpi}}_{\mathrm{A}}^{\mathrm{T}}(k)\boldsymbol{\vartheta}_{\mathrm{A}}(k) + \frac{1}{2} R^{-1} \boldsymbol{\alpha} \nabla \boldsymbol{\vartheta}_{\mathrm{C}}^{\mathrm{T}}(k) \hat{\boldsymbol{\varpi}}_{\mathrm{C}}(k)\right)^{\mathrm{T}} \end{cases} \tag{52}$$

where the index operator $\Delta_\Omega(k)$ denotes whether the enabled event happens or not, which is determined by conditions (52), and $\boldsymbol{u}^{\text{opt}}$ is the optimal voltage vector.

Remark 6: It is noticeable that if $\Delta_\Omega(k) = 1$, then the event is enabled. It means that the system trajectory crosses the defined threshold. If $\Delta_\Omega(k) = 0$, then the event is not enabled. The iteration optimization process will be suspended, and the modified weight update laws and the control input are held as constant. To be more precise, by monitoring a feedback from the robust data-driven MPC controller to enable the event, a user-predesigned threshold δ_e is detected and used to decide when necessary to solve the data-driven model-free RL control optimization problem. Thus, unnecessary triggering and switching commutation actions can be alleviated.

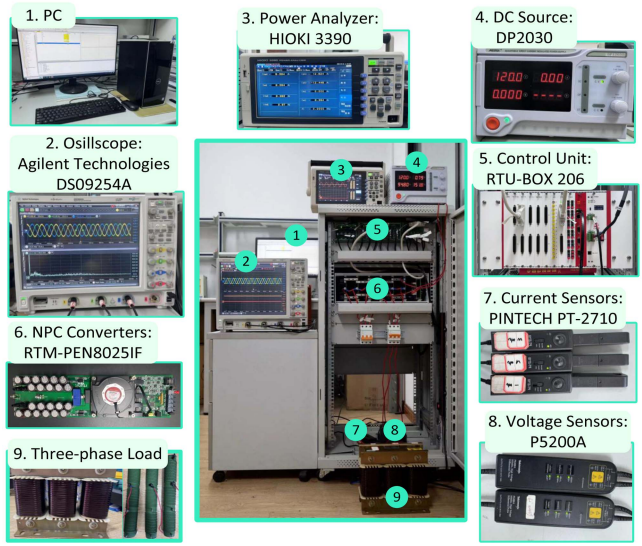

Fig. 3. Experimental platform of three-phase NPC converter system. 1) PC. 2) Osillscope: Agilent Technologies DS09254 A. 3) Power analyzer: HIOKI 3390. 4) DC source: DP2030. 5) Control unit: RTU-BOX 206. 6) NPC converters: RTM-PEN8025IF. 7) Current sensors: PINTECH PT-2710. 8) Voltage sensors: P5200 A. 9) Three-phase load: Three-phase RL load. For the implementation of this test, the real NPC converters prototype using the RTM-PEN8025IF modules is controlled, and the controller utilizes an RTU-BOX206 real-time digital control unit that includes a TMS320C28346 DSP from Texas Instrument. This DSP is installed in a modular electronic system, where the pulsewidth modulation signals are generated by the field-programmable gate array circuit.

G. Capacitor-Less Voltage-Balancing Scheme

In this section, we introduce the capacitor-less voltage-balancing scheme to effectively avoid the tuning work of weighting factors [7]. Then, in order to determine the optimal switching state, this approach employs a two-stage selection mechanism: 1) The cost function in (51) is evaluated by all available 19 active voltage vectors. The vector that yields the minimum cost function value is determined as the optimal voltage vector. 2) For optimal large/medium vectors, their corresponding switching states are directly implemented without further modification. For optimal small/zero vectors, an additional cost function is applied by

$$\begin{cases} \mathcal{J}_{N,\text{small}} = \text{sgn}(v_{p,n}) \times \text{sgn}(i_O) \\ \mathcal{J}_{N,\text{zero}} = \|S_{g,abc}(k) - S_{g,abc}(k-1)\|_2^2 \end{cases} \tag{53}$$

where i_O is the neutral-point current. $\text{sgn}(\cdot) = \text{sgn}(\cdot) = (\cdot)/|\cdot|$ is the signum function. Furthermore, a delay compensation control technique in [31] is here introduced into this proposal for real-time control implementation.

IV. Case Study

A. Control Implementation

This section depicts the test bench and shows the simulation and experimental results. As can be appreciated in Fig. 3, the experimental platform of the controlled system is given,

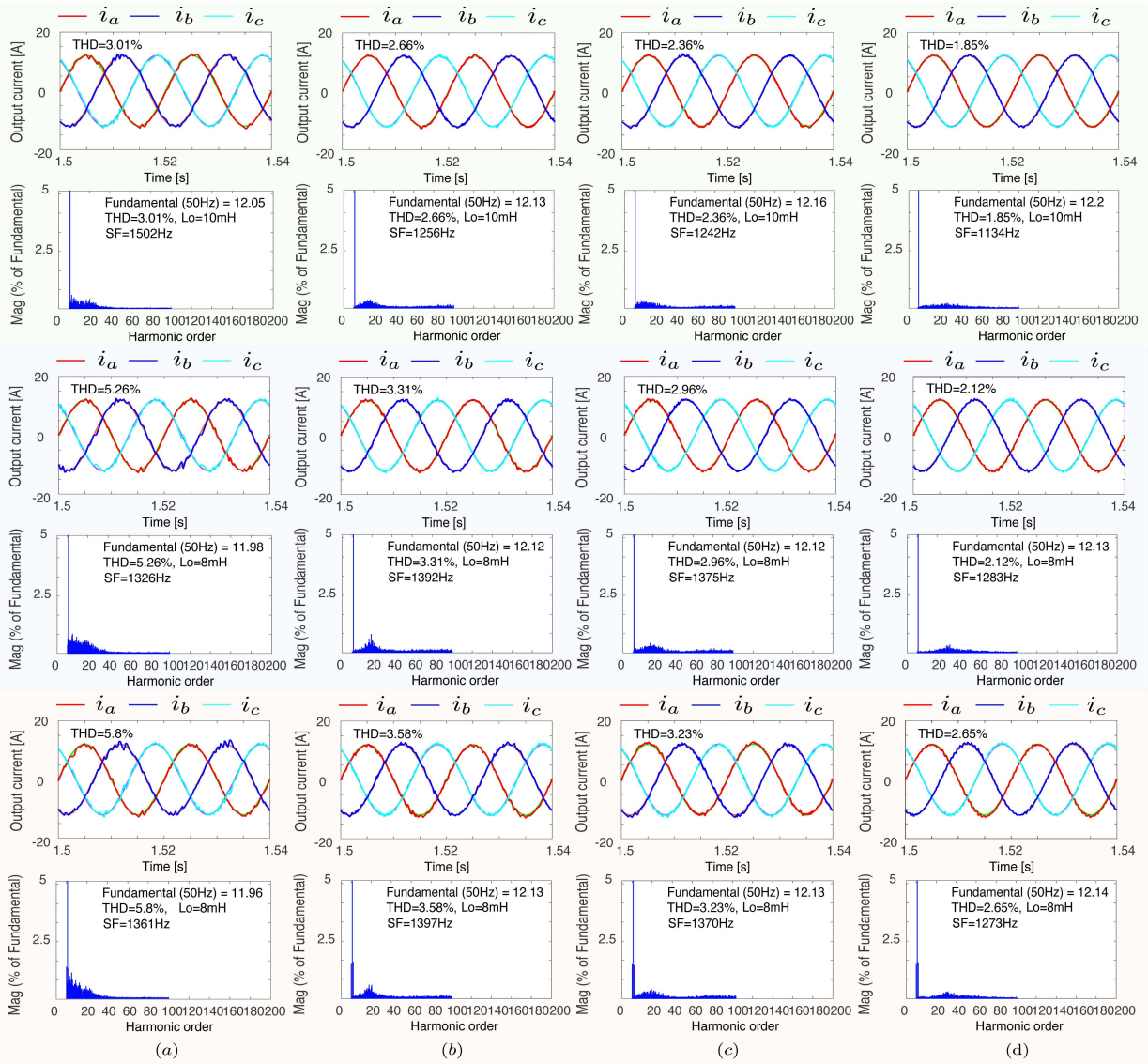

Fig. 4. Performance evaluation with four different FCS-MPC solutions in steady state. (I) Under normal operation. (II) Under parameter mismatch condition. (III) Under both parameter mismatch and external disturbances conditions. (a) ET-based FCS-MPC method. (b) ETESO-based FCS-MPC method. (c) ETPNN-based FCS-MPC method. (d) Proposed FCS-MPC solution.

comprising some photos. In our control setup, the real NPC converter prototype leveraging RTM-PEN8025IF modules is controlled by a system, including an RTU-BOX206 real-time digital controller. This controller incorporates a Texas Instrument TMS320C28346 digital signal processor (DSP) as its core component. Before performing the test, the same parameters are set. The load resistance and inductance are 0.5Ω and 10 mH, respectively. The dc-link voltage is 120 V. The dc-link capacitor is 2700 μF. The sampling/control period is 100 μs. Note that we assume that external disturbances occur, the signal is defined as $\mathbf{\Gamma}(\boldsymbol{x}) = \mathrm{A}_m(1+\boldsymbol{x})\sin(\mathrm{B}_m\pi t)$ and is injected into the sensor of controlled plant, where $\mathrm{A}_m = 0.03$ denotes the disturbance amplitude and $\mathrm{B}_m = 100$ denotes the disturbance frequency. The user-predesigned parameters are set as $\eta_\alpha = 20$, $\eta_\beta = 0.1$, $\gamma_A = 0.05$, $\gamma_B = 0.025$, $\gamma_C = 0.0025$, $\gamma_D = 0.01$, $\gamma_E = 0.01$, $\lambda_C = 1e^{-4}$, and $\lambda_D = 0.001$, respectively.

B. Simulation Result Analysis

In this section, the representative simulation results are provided to verify the feasibility of our proposed solution. Notably, Fig. 4 clearly demonstrates the output current waveforms and harmonic performance analysis of four different control approaches under normal operation, parameter mismatch, and external disturbance conditions. As shown in figure, output currents under normal operation exhibit the total harmonic distortion (THD) values as 3.01%, 2.66%, 2.36%, and 1.85%, respectively. Under parameter mismatch (from $L_o = 10$ mH to $L_o = 8$ mH), the waveform quality indices of output currents are 5.26%, 3.31%, 2.96%, and 2.12%, respectively. In addition, the THD values under both parameter mismatch and external disturbance conditions are 5.8%, 3.58%, 3.23%, and 2.65%, respectively. Noticeably, this is recognized as one of the critical

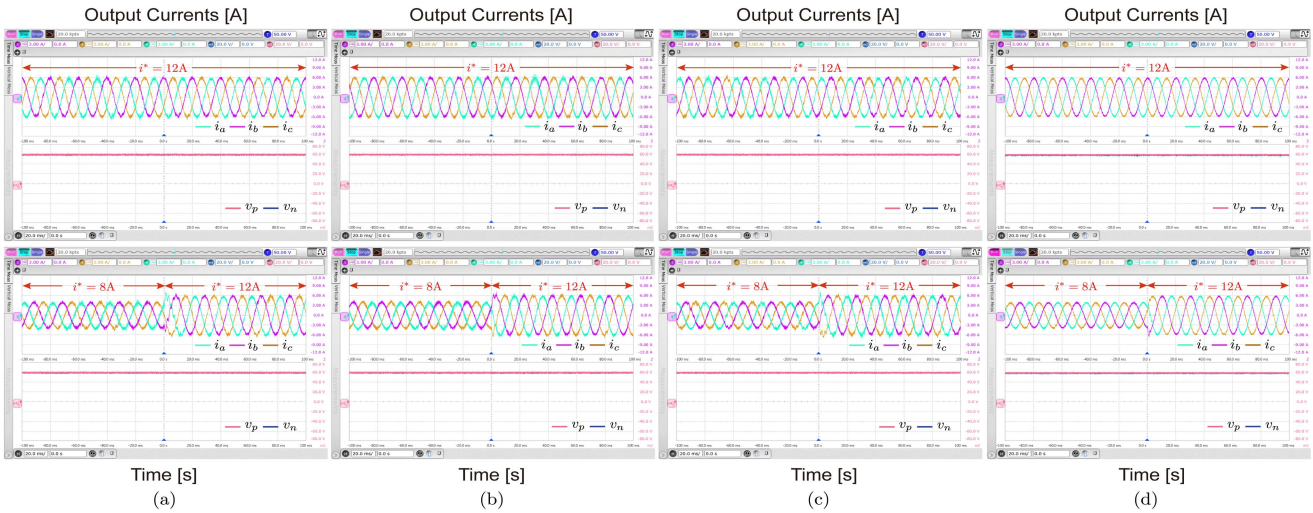

Fig. 5. Experimental results of three-phase 3L-NPC converter system with steady-state and transient-state performances under both unknown perturbations and parameter mismatch conditions. (a) ET-based FCS-MPC method. (b) ETESO-based FCS-MPC method. (c) ETPNN-based FCS-MPC method. (d) Proposed FCS-MPC solution.

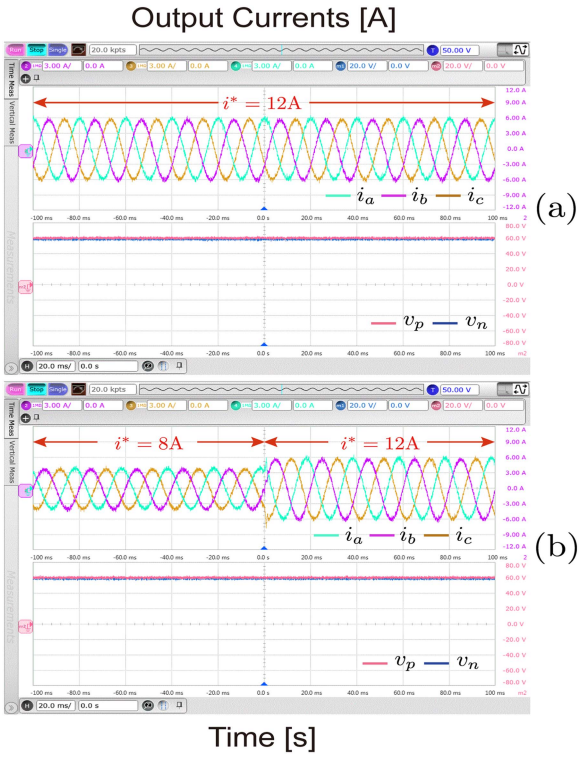

Fig. 6. Performance evaluation with the proposed FCS-MPC approach under parameter mismatch condition ($L_o = 5$ mH). (a) Output currents: steady-state performance. (b) Output currents: transient-state performance.

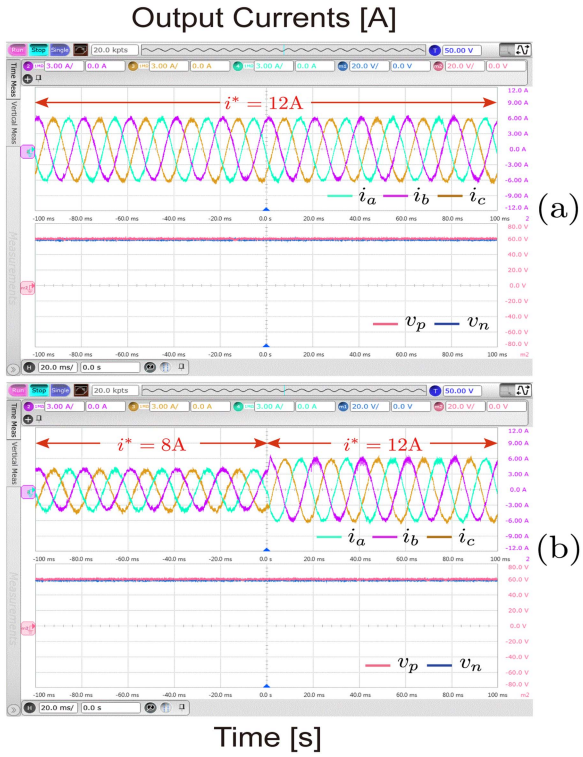

Fig. 7. Performance evaluation with the proposed FCS-MPC approach under external disturbance condition. (a) Output currents: steady-state performance. (b) Output currents: transient-state performance.

worst case scenarios in power converter operation. By comparison, our proposal achieves the desired control behavior, which can be seen from the output current waveforms in Fig. 4. This confirms the availability of the proposed control strategy, which not only overcomes the inherent restrictions of high SF and parameter uncertainties but also enhances performance under both low SF operation and external disturbances conditions.

C. Experimental Result Analysis

Next, to validate our findings and highlight the applicability and adaptability of the proposed method, the control behavior of the enhanced data-driven FCS-MPC scheme is demonstrated through experimental testing. The objective is to assess its performance under various practical conditions, including both parameter uncertainties and external disturbances, resembling one of the worst case operational scenarios. First of all, Fig. 5

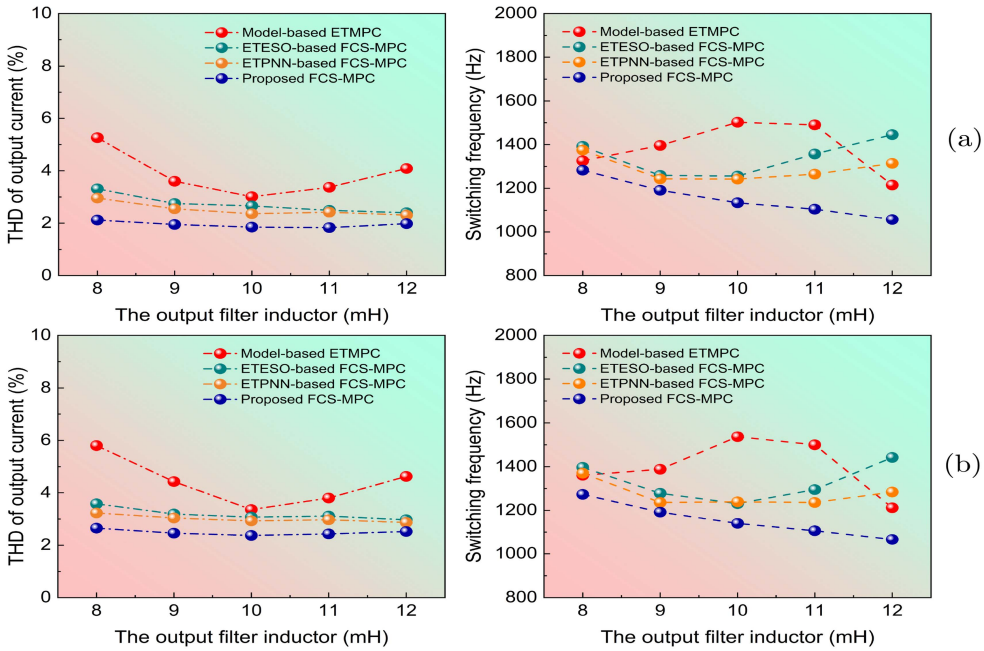

Fig. 8. Performance evaluation with four different FCS-MPC approaches. (a) Effect of THD and SF under parameter mismatch condition. (b) Effect of THD and SF under both parameter mismatch and external disturbances conditions.

TABLE II
COMPARISON RESULTS BETWEEN SEVEN DIFFERENT CONTROL SCHEMES

Control method	**Execution time** (μs) Algorithm optimization process	**THD** (%) Match/Mismatch/ Mismatch + Disturbances	**Average SF** (Hz) Match/Mismatch/ Mismatch + Disturbances	**Tracking error** (%) Match/Mismatch/ Mismatch + Disturbances
ET-based FCS-MPC method	50.5	3.01/5.26/5.8	1502/1326/1361	4.134/4.197/4.674
ETESO-based FCS-MPC method	78.6	2.66/3.31/3.58	1256/1392/1397	2.247/2.862/3.341
ETPNN-based FCS-MPC method	83.3	2.36/2.96/3.23	1242/1375/1370	2.346/2.578/3.098
ET-based EPH-FCS-MPC method	26.7	2.93/4.23/4.52	1132/1420/1403	3.952/4.272/4.346
Two-stage ET-MFPC method	89.6	1.39/2.72/3.07	1278/1384/1388	1.345/2.372/3.031
Learning MFPC method	65.9	1.57/2.32/2.75	1284/1211/1223	3.284/3.028/3.582
Proposed FCS-MPC solution	88.7	1.85/2.12/2.65	1134/1283/1273	2.435/2.213/2.843

depicts the control performance and output current response characteristics. Meanwhile, the performance assessment of the proposed control strategy under varying load conditions (from $L_o = 10$ mH to 5 mH) has also been presented, as illustrated in Fig. 6. As expected, the proposed approach achieves outstanding control performance in terms of output current waveforms. In addition, it can be observed that the dc-link capacitor voltages are effectively regulated to their nominal values using a capacitorless voltage-balancing control strategy. The suggested control design operates without requiring prior knowledge of the system mathematical model, successfully achieving the desired control objectives while enhancing performance under both parameter uncertainty and external disturbance conditions.

On the other hand, data-driven predictive control leverages historical data to build accurate predictive models, facilitating informed decision-making. In practical implementation, however, precise data is usually unavailable due to measurement noise and input noise. It is noteworthy that this issue results in imprecise estimations and predictions, and may ultimately deteriorate the control performance. It can be assumed that external disturbances arise from unavoidable noise in state measurements. The noise signal is defined as $\mathbf{\Gamma}(\boldsymbol{x}) = \mathrm{A}_m(1 + \boldsymbol{x})\sin(\mathrm{B}_m \pi t)$, and is injected into the sensor of the controlled plant. Here, A_m denotes the signal amplitude, which is set to 0.03, while B_m stands for the signal frequency, selected as 200 (see Fig. 7 for details). In this literature, the injection of the noise signal $\mathbf{\Gamma}(\boldsymbol{x})$ into the controlled plant's sensor causes incorrect control decisions to be transmitted to the power converter. As depicted in Fig. 7, this phenomenon may not only trigger potential equipment damage but also exert a negative influence on the control performance of power converter systems. To overcome this defect, we take into account to compensate for the uncertainties in the system model, and consequently, the desired control performance under different load conditions can be guaranteed as anticipated.

D. Robustness Performance Analysis

In this section, the performance of four different FCS-MPC solutions under both parameter mismatch and external disturbances scenarios is assessed in detail. The obtained results are summarized in Fig. 8, where the desired harmonic and robust performance as well as low SF can be achieved by utilizing this proposal. Meanwhile, a summary of the comparative results for the different formulations is given in Table II. The results demonstrate that the proposed FCS-MPC framework

significantly outperforms other state-of-the-art ET-based MPC methods by leveraging the AI-driven and data-driven as well as event-driven schemes in the context of power converter systems, while maintaining a lower SF under both parameter mismatch and external disturbances scenarios.

V. Conclusion and Future Research Directions

This article was concerned with a remarkably flexible control framework that integrates a PI-like data-driven DIMPC and an RL technique as well as variable-step event-driven mechanism so as to enhance the performance and reject both model mismatch and unknown disturbances. Specifically, the distinctive features of this proposal lay in its superior disturbance attenuation and tracking capability, robustness against parameter variations, and good regulation properties under low SF scenario. In conclusion, we demonstrated our theoretical findings and emphasized its advantages over state-of-the-art low SF-based FCS-MPC approaches. The results indicated that our modification was capable of effectively taking the model parameter mismatch and unknown uncertainties into account.

We believe that this method presents a few clear avenues for future work, and can be extended to other converter topologies (e.g., modular multilevel and boost converters) or control scenarios (e.g., current versus voltage mode). To be more precise, a potential research avenue for future work involves extending the proposed refinement to integrate a wider spectrum of power converter/motor control systems and devoting the improvement of performance with the help of digital twin technique [32], [33].

Despite the contributions of this work, many open issues remain that future research is going to investigate. First, there is the extension of the data-driven MFPC frameworks, where challenges, such as the selective harmonic elimination technique and potentially computational burden, have to be addressed [34], [35]. While the real-world experiments have indicated that this proposal can also deal with measurement noise and parametric uncertainties, future research is going to study theoretically and by thorough experiments to which extent this suggested control solution can solve malicious attack issues in power converter system [36].

Acknowledgment

The authors would like to thank the Editor-in-Chief, Associate Editor, and anonymous referees for their invaluable comments and suggestions, which greatly helped us to significantly enhance the quality of this article.

References

[1] S. Vazquez, J. Rodríguez, M. Rivera, L. G. Franquelo, and M. Norambuena, "Model predictive control for power converters and drives: Advances and trends," *IEEE Trans. Ind. Electron.*, vol. 64, no. 2, pp. 935–947, Feb. 2017.

[2] S. Vazquez et al., "Model predictive control: A review of its applications in power electronics," *IEEE Ind. Electron. Mag.*, vol. 8, no. 1, pp. 16–31, Mar. 2014.

[3] Y. Zhang, J. Jin, and L. Huang, "Model-free predictive current control of PMSM drives based on extended state observer using ultralocal model," *IEEE Trans. Ind. Electron.*, vol. 68, no. 2, pp. 993–1003, Feb. 2021.

[4] B. Long, J. Zhang, D. Shen, J. Rodríguez, J. M. Guerrero, and K. T. Chong, "Ultralocal model-free predictive control of T-type grid-connected converters based on extended sliding-mode disturbance observer," *IEEE Trans. Power Electron.*, vol. 38, no. 12, pp. 15494–15508, Dec. 2023.

[5] P. G. Carlet, A. Favato, S. Bolognani, and F. Dörfler, "Data-driven continuous-set predictive current control for synchronous motor drives," *IEEE Trans. Power Electron.*, vol. 37, no. 6, pp. 6637–6646, Jun. 2022.

[6] F. Wang, Y. Wei, J. Rodríguez, and C. Garcia, "State-of-art, development, and challenges of model-free predictive control on motor drives," *IEEE Trans. Power Electron.*, vol. 40, no. 8, pp. 10846–10864, Aug. 2025.

[7] W. Wu, L. Qiu, X. Liu, J. Ma, J. Rodríguez, and Y. Fang, "Dynamic-linearization-based predictive control of a voltage source inverter," *IEEE Trans. Ind. Electron.*, vol. 71, no. 4, pp. 3275–3284, Apr. 2024.

[8] X. Liu, L. Qiu, Y. Fang, and J. Rodríguez, "Predictor-based data-driven model-free adaptive predictive control of power converters using machine learning," *IEEE Trans. Ind. Electron.*, vol. 70, no. 8, pp. 7591–7603, Aug. 2023.

[9] X. Zhang, Z. Ma, H. Niu, J. Huang, and G. Lin, "Finite-control-set model-predictive control with data-driven switching frequency control for single-phase three-level NPC rectifiers," *IEEE Trans. Ind. Electron.*, vol. 71, no. 7, pp. 7180–7189, Jul. 2024.

[10] Y. Huang, A. Chen, T. Liu, Q. Ren, Y. Cui, and H. Tang, "Data-driven predictive control for grid-forming inverters with enhanced voltage performance in islanded operation based on full-form dynamic-linearization," *IEEE Trans. Ind. Electron.*, vol. 72, no. 11, pp. 11239–11249, Nov. 2025.

[11] Y. Huang and X. Zhao, "Reinforcement learning-based multiobjective control of grid-connected wind farms," *IEEE Trans. Ind. Informat.*, vol. 20, no. 5, pp. 7380–7390, May 2024.

[12] T. T. Nguyen, H. N. Tran, T. H. Nguyen, and J. W. Jeon, "Recurrent neural network-based robust adaptive model predictive speed control for PMSM with parameter mismatch," *IEEE Trans. Ind. Electron.*, vol. 70, no. 6, pp. 6219–6228, Jun. 2023.

[13] C. Zhang, H. Wang, X. Yuan, and X. Wu, "Optimized fuzzy model predictive torque control with a dynamic flux weighting factor for nine-phase open-end winding PMSMs," *IEEE Trans. Emerg. Sel. Topics Power Electron.*, vol. 13, no. 2, pp. 2385–2396, Apr. 2025.

[14] Z. Gong, P. Tuo, C. Zheng, and X. Wu, "Design and analysis of the model predictive control implemented by the ANN technique for MMC-based rectifier with improved grid adaptability," *IEEE Trans. Power Electron.*, vol. 39, no. 10, pp. 12306–12322, Oct. 2024.

[15] C. Liu, J. Ma, X. Liu, L. Qiu, W. Wu, and Y. Fang, "A predictive control method based on neural predictor and soft actor-critic for power converters," *IEEE Trans. Ind. Electron.*, vol. 72, no. 5, pp. 4556–4566, May 2025.

[16] Y. Wan, Q. Xu, and T. Dragičević, "Reinforcement learning-based predictive control for power electronic converters," *IEEE Trans. Ind. Electron.*, vol. 72, no. 5, pp. 5353–5364, May 2025.

[17] Y. Wan, Y. Zhang, and Q. Xu, "Computationally efficient long-horizon predictive control for power converter: A reinforcement learning approach," *IEEE Trans. Ind. Electron.*, vol. 72, no. 10, pp. 10814–10825, Oct. 2025.

[18] X. Liu, L. Qiu, Y. Fang, K. Wang, Y. Li, and J. Rodríguez, "Predictive control of voltage source inverter: An online reinforcement learning solution," *IEEE Trans. Ind. Electron.*, vol. 71, no. 7, pp. 6591–6600, Jul. 2024.

[19] A. Edpuganti and A. K. Rathore, "A survey of low switching frequency modulation techniques for medium-voltage multilevel converters," *IEEE Trans. Ind. Appl.*, vol. 51, no. 5, pp. 4212–4228, Sep./Oct. 2015.

[20] B. Wang et al., "Event-triggered model predictive control for power converters," *IEEE Trans. Ind. Electron.*, vol. 68, no. 1, pp. 715–720, Jan. 2021.

[21] X. Liu et al., "Event-triggered ESO-based robust MPC for power converters," *IEEE Trans. Ind. Electron.*, vol. 70, no. 2, pp. 2144–2152, Feb. 2023.

[22] X. Liu et al., "Event-triggered neural predictor-based FCS-MPC for MMC," *IEEE Trans. Ind. Electron.*, vol. 69, no. 6, pp. 6433–6440, Jun. 2022.

[23] X. Liu, L. Qiu, Y. Fang, K. Wang, Y. Li, and J. Rodríguez, "Combining data-driven and event-driven for online learning predictive control in power converters," *IEEE Trans. Power Electron.*, vol. 40, no. 1, pp. 563–573, Jan. 2025.

[24] J. Luo, Y. Luo, K. Yang, M. S. Hossen, and J. Yu, "Dynamic threshold adjustment-based event-triggered model predictive control for PMSM motor," *IEEE Trans. Power Electron.*, vol. 40, no. 11, pp. 16206–16218, Nov. 2025.

[25] Z. F. Lin et al., "A model-independent online learning-based control strategy for DC/AC inverters," *IEEE Trans. Power Electron.*, vol. 41, no. 1, pp. 169–173, Jan. 2026.

[26] Y. Shen, Z. Yin, F. Zhou, Y. Zhang, X. Wang, and H. Zhao, "Tiny neural network-based ultra-local model-free predictive control for PMSMs," *IEEE Trans. Power Electron.*, vol. 41, no. 1, pp. 132–136, Jan. 2026.

[27] R. Chi, Y. Hui, S. Zhang, B. Huang, and Z. Hou, "Discrete-time extended state observer-based model-free adaptive control via local dynamic linearization," *IEEE Trans. Ind. Electron.*, vol. 67, no. 10, pp. 8691–8701, Oct. 2020.

[28] J. Na, Y. Lv, K. Zhang, and J. Zhao, "Adaptive identifier-critic-based optimal tracking control for nonlinear systems with experimental validation," *IEEE Trans. Syst., Man, Cybern., Syst.*, vol. 52, no. 1, pp. 459–472, Jan. 2022.
[29] J. Duan, Z. Yi, D. Shi, C. Lin, X. Lu, and Z. Wang, "Reinforcement-learning-based optimal control of hybrid energy storage systems in hybrid AC-DC microgrids," *IEEE Trans. Ind. Informat.*, vol. 15, no. 9, pp. 5355–5364, Sep. 2019.
[30] D. Wang, N. Gao, D. Liu, J. Li, and F. L. Lewis, "Recent progress in reinforcement learning and adaptive dynamic programming for advanced control applications," *IEEE-CAA J. Automatica Sinica*, vol. 11, no. 1, pp. 18–36, Jan. 2024.
[31] P. Cortés, J. Rodríguez, C. Silva, and A. Flores, "Delay compensation in model predictive current control of a three-phase inverter," *IEEE Trans. Ind. Electron.*, vol. 59, no. 2, pp. 1323–1325, Feb. 2012.
[32] C. Wu, Z. Cui, Q. Xia, J. Yue, and F. Lyu, "An overview of digital twin technology for power electronics: State-of-the-art and future trends," *IEEE Trans. Power Electron.*, vol. 40, no. 9, pp. 13337–13362, Sep. 2025.
[33] R. Torchio et al., "Digital twins in power electronics: A comprehensive approach to enhance virtual thermal sensing," *IEEE Trans. Power Electron.*, vol. 40, no. 5, pp. 6977–6987, May 2025.
[34] Z. Zhang, G. Chen, and D. Xu, "Harmonic programmed modulation for high-power medium voltage energy conversion: Formulation, solving approach, and implementation," *IEEE Trans. Power Electron.*, vol. 40, no. 6, pp. 7872–7892, Jun. 2025.
[35] O. Babayomi, Y. Li, Z. Zhang, and K.-B. Park, "Advanced control of grid-connected microgrids: Challenges, advances, and trends," *IEEE Trans. Power Electron.*, vol. 40, no. 6, pp. 7681–7708, Jun. 2025.
[36] Z. Zhang, J. Hu, J. Lu, J. M. Guerrero, and J. Cao, "Dynamic defense method against malicious attacks for DC microgrids," *IEEE Trans. Power Electron.*, vol. 40, no. 7, pp. 9591–9605, Jul. 2025.

Xing Liu (Senior Member, IEEE) received the Ph.D. degree in marine electric engineering from Dalian Maritime University, Dalian, China, in 2018.

From 2018 to 2019, he joined the Key Laboratory of Marine Technology and Control Engineering of the Ministry of Communications, Shanghai Maritime University, Shanghai, China. He is currently a Professor with the College of Electrical Engineering, Shanghai Dianji University, Shanghai. He is also a Research Fellow with the State Key Laboratory of High-Speed Maglev Transportation Technology, Qingdao, China. He is also a Research Fellow with the State Key Laboratory of Power Transmission Equipment Technology, Chongqing University, Chongqing, China. He is also a Research Fellow with the College of Electrical Engineering, Zhejiang University, Hangzhou, China. He is also currently a Visiting Scholar in the area of high-power converters and renewable energy generation with the Department of Electrical Engineering, Tsinghua University, Beijing, China. He has authored more than 35 TOP publications, all of which are the first authors, including papers in prestigious journal, such as IEEE TRANSACTIONS ON INDUSTRIAL ELECTRONICS, IEEE TRANSACTIONS ON POWER ELECTRONICS, IEEE TRANSACTIONS ON TRANSPORTATION ELECTRIFICATION, IEEE TRANSACTIONS ON CONTROL SYSTEMS TECHNOLOGY, IEEE TRANSACTIONS ON MECHATRONICS, IEEE JOURNAL OF EMERGING AND SELECTED TOPICS IN POWER ELECTRONICS, *ISA Transactions*, and *International Journal of Electrical Power and Energy Systems*. His research interests include finite control-set model predictive control and data-driven predictive control of power converter control systems with applications in power grids, microgrids, and power electronics converters, cybersecurity of power-electronic-intensive electrical distributions systems and microgrids, and applications of artificial intelligence in industrial power electronics and systems.

Lin Qiu (Senior Member, IEEE) received the B.S. and Ph.D. degrees in electrical engineering from the Department of Electrical Engineering, Tsinghua University, Beijing, China, in 2011 and 2017, respectively.

He is currently a Research Professor with the Zhejiang University-University of Illinois at Urbana-Champaign Institute, Zhejiang, China. His current research interests include transportation electrification, grid resilience enhancement, and data-driven system control algorithm.

Youtong Fang (Senior Member, IEEE) received the B.S. and Ph.D. degrees in electrical engineering from the Hebei University of Technology, Tianjin, China, in 1984 and 2001, respectively.

He is currently a Professor with the College of Electrical Engineering, Zhejiang University, Hangzhou, China. His research interests include the application, control, and design of electrical machines.

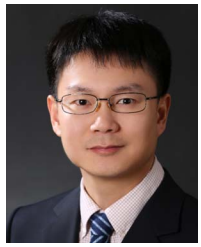

Kui Wang (Senior Member, IEEE) was born in Hubei, China, in 1984. He received the B.S. and Ph.D. degrees in electrical engineering from the Department of Electrical Engineering, Tsinghua University, Beijing, China, in 2006 and 2011, respectively.

From 2018 to 2019, he was a Visiting Scholar with the Center for Ultrawide-area Resilient Electric Energy Transmission Networks, University of Tennessee, Knoxville, TN, USA. He is currently an Associate Researcher with the Department of Electrical Engineering, Tsinghua University. His research interests include topology and control of multilevel converters, renewable energy generation, and wide band-gap semiconductor applications.

Dr. Wang was recognized as the 2022 Distinguished Reviewer for IEEE TRANSACTIONS ON POWER ELECTRONICS and IEEE TRANSACTIONS ON INDUSTRIAL ELECTRONICS.

Yongdong Li (Senior Member, IEEE) was born in Hebei, China, in 1962. He received the B.S. degree from the Harbin Institute of Technology, Harbin, China, in 1982, and the M.S. and Ph.D. degrees from the Department of Electrical Engineering, Institute National Polytechnique de Toulouse, Toulouse, France, in 1984 and 1987, respectively, all in electrical engineering.

He was an Invited Professor with the Institute National Polytechnique de Toulouse and the Dean of the School of Electrical Engineering, Xinjiang University, Urumchi, China. Since 1996, he has been a Professor with the Department of Electrical Engineering, Tsinghua University, Beijing, China. He is also the Lead Developer of the Power Electronics and Motor Control Laboratory, Tsinghua University. His current research interests include power electronics, machine control, and wind power generation.

Dr. Li is a Senior Member of the China Electro-Technique Society, the Vice President of the China Power Electronics Society, and the Vice President of the Electrical Automation Committee of China Automation Association.

José Rodríguez (Life Fellow, IEEE) received the Engineering degree in electrical engineering from the Universidad Tecnica Federico Santa Maria, Valparaiso, Chile, in 1977, and the Dr.-Ing. degree in electrical engineering from the University of Erlangen, Erlangen, Germany, in 1985.

He has been with the Department of Electronics Engineering, Universidad Tecnica Federico Santa Maria, since 1977, where he was a Full Professor and President. Since 2015 to 2019, he was the President of Universidad Andres Bello, Santiago, Chile. From 2022 to 2023, he was a President of Universidad San Sebastian, Santiago, Chile. Now, he is the Director of the Center for Energy Transition, Universidad San Sebastian. He has coauthored two books, several book chapters, and more than 1000 journal and conference papers. His research interests include multilevel inverters, new converter topologies, control of power converters, and adjustable-speed drives.

Dr. Rodríguez was the recipient of a number of best paper awards from journals of the IEEE, the National Award of Applied Sciences and Technology from the government of Chile in 2014, and the Eugene Mittelmann Award from the Industrial Electronics Society of the IEEE in 2015. He is a Member of the Chilean Academy of Engineering. From 2014 to 2024, he was included in the list of Highly Cited Researchers published by Web of Science.